Geophys. J. Int. (1993) **114**, 249–272

Constraining upper mantle anelasticity using surface wave amplitude anomalies

Joseph J. Durek,[1] Michael H. Ritzwoller[2] and John H. Woodhouse[3]

[1] *Department of Earth and Planetary Sciences, Harvard University, Cambridge, MA* 02138, *USA*
[2] *Department of Physics, University of Colorado, Box* 390, *Boulder, CO* 80309-0390, *USA*
[3] *Department of Earth Sciences, Oxford University, Parks Road, Oxford* OX1 3PR, *UK*

Accepted 1992 December 8. Received 1992 October 5; in original form 1992 March 1

SUMMARY

We present an iterative method to constrain lateral variations in surface wave attenuation using long-period surface wave amplitude anomalies. The method acts to isolate the anelastic signal from elastic focusing effects, yielding largely unbiased estimates of lateral variations in the inverse seismic quality factor, $q(\omega) = Q^{-1}(\omega)$, of the surface wave. In the zeroth iteration, linearized ray theory motivates the construction of a reduced datum, using measurements from four consecutive surface wave orbits, which is insensitive to elastic heterogeneity, an operation which requires no *a priori* knowledge of elastic structure. Synthetic experiments using both ray theoretic formalisms and normal-mode calculations reveal that significant levels of elastic bias remain in the reduced data due to deviations from linearized ray theory. In further efforts to eliminate elastic bias, the remaining elastic signal in each reduced datum is predicted and subtracted using accurate forward theory and existing aspherical elastic mantle models. This operation is the first iteration of a non-linear inversion in which the data at each iteration are the residuals between the observed anomalies and the anomalies predicted for a fixed phase velocity model and updated attenuation model.

The zeroth and first iterations are performed with 1610 vertical and 790 longitudinal component seismograms from 144 events. Heterogeneity maps of Rayleigh wave attenuation $\delta q(\omega, \theta, \phi)$ are retrieved for the even degrees 2, 4 and 6 of a spherical harmonic expansion in the period range of 150–300 s ($_0S_{25} - {}_0S_{60}$). These surface wave attenuation maps are analogous to elastic phase velocity in their radial averaging of, and linear relationship to, intrinsic heterogeneity and are inverted for upper mantle anelastic structure. Under the physically plausible assumption that intrinsic elastic and anelastic structure are correlated at every depth, the surface wave attenuation maps are well explained by a source region of anelastic heterogeneity that is radially localized in the shallow mantle (100–300 km) in a region we infer to be near the solidus temperature.

Key words: anelasticity, attenuation, inversion, surface waves, upper mantle.

1. INTRODUCTION

In this study, we constrain long-wavelength lateral variations in surface wave attenuation in the upper mantle using amplitude anomalies of multiply orbiting surface waves. The lateral variations in the inverse quality factor $q(\omega) = Q^{-1}(\omega)$ of the surface wave represent a weighted radial average of intrinsic anelastic structure (Woodhouse & Dahlen 1978) and are used in a preliminary inversion to locate the 3-D distribution of anelastic heterogeneity in the upper mantle.

Amplitude and phase anomalies observed in long-period surface waves are well understood in character, if not in detail. Because of the robust relationship between phase anomaly observations and elastic structure, the understanding of the mantle's velocity structure has advanced appreciably. Numerous velocity models exist for the upper mantle (e.g. Masters *et al.* 1982; Nakanishi & Anderson 1983,

1984; Woodhouse & Dziewonski 1984; Tanimoto 1985, 1986; Romanowicz, Roult & Kohl 1987; Ritzwoller, Masters & Gilbert 1988) based on the modelling of seismic phases as either traveltime anomalies or eigenfrequency shifts. Recent investigations have incorporated amplitude anomalies and modelled elastic focusing effects to provide tighter constraints on upper mantle elastic structure (Pollitz, Park & Dahlen 1987; Wong 1989). However, while existing elastic models successfully explain anomalies in phase, only a small fraction of the observed amplitude anomalies are properly predicted and much of the amplitude signal remains unmodelled. A prominent additional source of the observed amplitude anomalies is aspherical variation in the dissipation, or attenuation, of surface waves in the mantle.

Attenuation studies have struggled with the ambiguity involved in the estimation of the seismic quality factor, since amplitude anomalies contain significant signal besides that attributable to anelastic dissipation. Surface wave amplitude anomalies are subject to uncertainties in the instrument response and seismic source, interference by overtone signals and, most importantly, the refraction of wave energy through elastic structure. Early observational studies of surface wave attenuation using amplitude measurements (Ben-Menahem 1965; Kanamori 1970) were unable to discern coherent lateral variations in the quality factor even though phase velocities were clearly seen to vary across regions of tectonic activity and quiescence. The measured phase-velocity variations were on the order of 1–2 per cent, but the inferred seismic quality factor varied by roughly 50 per cent. Later studies attempted to constrain a regionalized component in the variations of surface wave attenuation. Mills (1978) and Nakanishi (1979a) both used a 'pure-path' technique to study Rayleigh waves and observed a correlation between phase velocity and Q perturbations across certain tectonic regions. Dziewonski & Steim (1982) inferred a Q difference between continents and oceans consistent with the results of Sipkin & Jordan (1980) based on measurements of *ScS* attenuation. Roult (1982) also noted a correlation between low Q values and large path fraction across young ocean. Attempts have also been made to interpret observations of both normal mode multiplet peak widths and amplitudes in terms of aspherical Q. Davis (1985) showed that the variation of peak widths caused by realistic elastic structure and noise is approximately equal to the variation of attenuation signal and argued that the resolution of Q structure will be difficult from measurements of peak widths alone. Masters & Gilbert (1983) concluded that the distribution of apparent attenuation measurements from peak widths does not contain a coherent long-wavelength aspherical structure. Later, using a much larger data set of over 3000 recordings providing approximately 1200 measurements per multiplet, Smith & Masters (1989) reported the existence of a weak degree 2 aspherical-attenuation signal in peak widths which was negatively correlated with elastic-phase velocity. Romanowicz *et al.* (1987) fit degree 2 spherical harmonics to surface wave amplitude measurements and also reported a negative correlation with phase velocity. In further studies, Romanowicz, Ekström & Lognonné (1989) and Romanowicz (1990) sought to isolate the anelastic signal in a small number of high-quality amplitude anomalies and constrained low-degree variations in surface wave attenuation with a hypothesized source region at about 250–500 km depth.

To obtain unbiased measures of aspherical surface wave attenuation, the anelastic and elastic effects on seismic data must be distinguished. Optimally, the elastic and anelastic structure may be determined simultaneously using both amplitude and phase information. However, anelastic heterogeneity may also be recovered by isolating the anelastic signal in the amplitude data (Durek, Dziewonski & Woodhouse 1988; Durek, Ritzwoller & Woodhouse 1989; Romanowicz *et al.* 1989; Romanowicz 1990), keeping elastic signal from being mapped into, and therefore biasing, retrieved anelastic models. Motivating the initial step to isolate the anelastic signal, linearized ray theory, in which the linear effect of elastic focusing due to perturbations in phase velocity is calculated along the unperturbed great-circle path, suggests a recombination of observed amplitude anomalies that is desensitized to elastic structure. However, we will show that significant elastic signal remains in the data due to departures from linearized ray theory, leading to inferred attenuation maps that are biased by roughly 30 per cent in magnitude. To further isolate the anelastic signal, the remaining elastic bias in the data is estimated and removed using a fixed-reference elastic model. This operation represents the first iteration in the general iterative problem of estimating lateral variations in surface wave attenuation, where, at each iteration, the data comprise the residuals between the reduced amplitude anomalies and those predicted for an elastic reference model and the updated anelastic model. The retrieved coefficients describing lateral variations in surface wave attenuation are linear functionals of aspherical anelastic structure and can then be used as data in a linear inversion for intrinsic anelastic heterogeneity.

Section 2 details the iterative scheme to isolate and invert anelastic signal for variations in surface wave attenuation and reviews the general least-squares problem. In Section 3, data selection and data processing techniques are discussed. Section 4 presents the results of experiments where synthetic data have been used to estimate the potential bias caused by elastic signal. In Section 5, the models of aspherical attenuation for Rayleigh waves between 150–300 s is presented for the zeroth and first iterations. In the first iteration, both normal-mode theory and surface wave ray theory are used to remove remaining elastic signal. The results of the two techniques are compared. The inferences, both qualitative and quantitative, for the source region of anelastic heterogeneity are made in Section 6. The conclusions concerning intrinsic anelastic structure are robust and consistent for the first two iterations performed in this study.

2 INVERSE PROBLEM FOR SURFACE WAVE ATTENUATION

In this section, we investigate a datum in which the anelastic signal is desensitized to corrupting elastic signal and establish the non-linear inverse problem relating the datum to perturbations in surface wave attenuation.

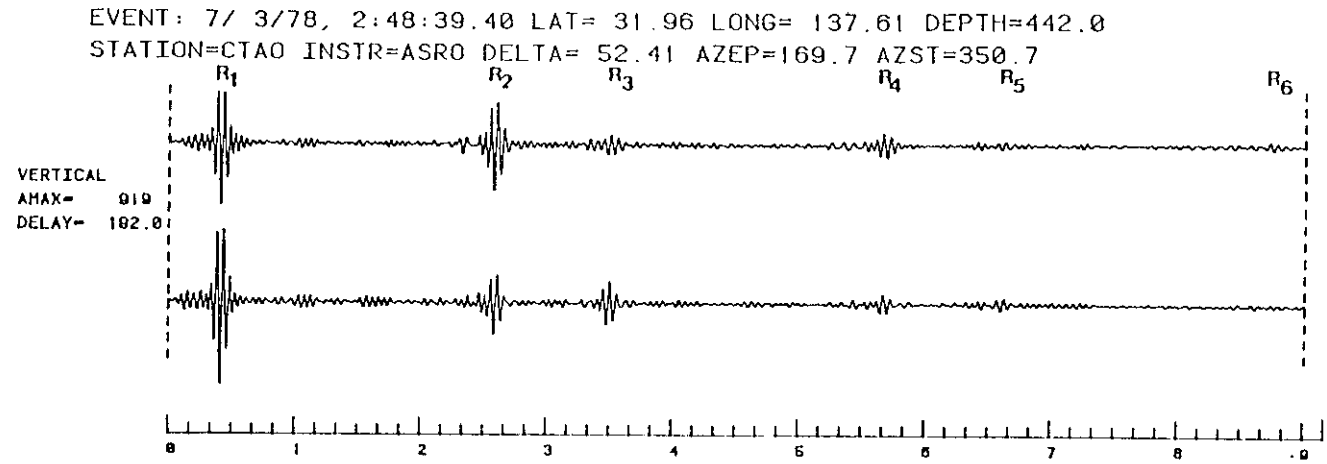

Figure 1. Comparison between observed seismogram (top) and synthetic seismogram (bottom) calculated from PREM demonstrating the effects of elastic focusing. In the data trace, even orbits ($n = 2, 4, \ldots$) are amplified with respect to the predicted trace while the odd orbits ($n = 1, 3, \ldots$) are deamplified [reproduced from Woodhouse & Wong (1986)].

2.1 Isolation of anelastic signal

Consider a multiply orbiting surface wave. The amplitude anomaly $a_n(\omega)$ for the nth surface wave orbit at frequency ω is defined as the ratio of the observed spectral amplitude of the orbit relative to that predicted by a spherical reference earth model,

$$a_n^{\text{obs}}(\omega) = A_n(\omega)/A_n^{\text{sph}}(\omega). \tag{1}$$

We seek to isolate the part of the observed amplitude anomaly attributable to aspherical attenuation in order to produce an unbiased relation between observable quantities and the anelastic model parameters, to be defined. If we consider the operator that maps the amplitude anomaly from one surface wavepacket arrival (R_n) to the next (R_{n+2}), the source and instrument uncertainty are cancelled, an advantage first advocated by Sato (1958). This operator involves the exponential decay of the wave along the path of the additional orbit travelled

$$\frac{a_{n+2}(\omega)}{a_n(\omega)} = \beta(\omega) \exp\left[\frac{-\omega}{2} \oint_{\text{orbit}} \delta q(\theta, \phi, \omega)\, dt\right], \tag{2}$$

where β denotes elastic focusing effects and δq is the spatial perturbation of the inverse quality factor of the surface wave at frequency ω. The quality factor of a surface wave is a function of the way in which the wave samples intrinsic anelastic structure and is therefore frequency dependent.

The seismograms in Fig. 1 demonstrate the necessity of addressing elastic focusing effects, showing a case in which the surface waves travelling in one direction are amplified relative to the theoretical seismogram, while waves travelling in the opposite direction are deamplified. This phenomenon cannot be explained by attenuation alone. Our efforts to reduce the elastic signal in the amplitude anomalies are motivated by the fact that anelasticity and elasticity influence amplitudes of oppositely travelling surface waves differently (Fig. 2). Elastic heterogeneity leads to focusing and amplification, for wave groups orbiting in one sense, and to defocusing and deamplification for those of the opposite sense (Woodhouse & Wong 1986). Anelastic heterogeneity, on the other hand, affects orbits of both

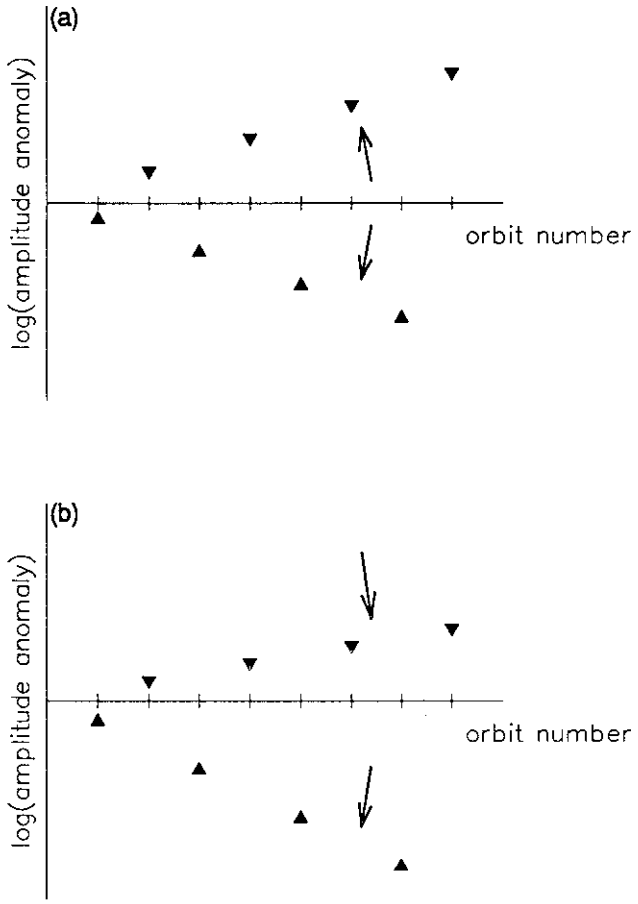

Figure 2. Qualitative plots of ln (amplitude anomaly) versus surface wave orbit number. (a) Elastic structure alone leads to focusing or defocusing depending on the direction of orbit. The case shown obeys linearized ray theory, where focusing and defocusing factors are reciprocals. (b) The introduction of anelastic heterogeneity uniformly suppresses amplitudes independent of the direction of orbit.

senses in a similar way. When the predictions of ray theory are linearized with respect to the aspherical phase-velocity perturbations it is found that orbits of one sense are

amplified (deamplified) by the same factor from orbit to orbit, and that those of the opposite sense are deamplified (amplified) by the reciprocal factor (Woodhouse & Wong 1986); we shall refer to this approximation as 'linearized ray theory'.

The first technique to reduce the biasing elastic signal is based on the differential behaviour of elastic and anelastic signals described by linearized ray theory. A datum d_n is constructed using ratios of amplitude anomalies from oppositely travelling waves over four consecutive orbits,

$$d_n = \frac{a_{n+2}}{a_n}\frac{a_{n+3}}{a_{n+1}}, \tag{3}$$

which, according to linearized ray theory, is completely insensitive to elastic structure (Durek *et al.* 1988, 1989; Romanowicz *et al.* 1989; Romanowicz 1990). The elastic signal is reduced without introducing any *a priori* knowledge of elastic structure. The resulting datum is referred to as *desensitized* to elastic structure. While it will be shown that departures from linearized ray theory result in a datum still appreciably biased by elastic signal, the procedure is valuable in that it does reduce elastic signal in the estimator for wave attenuation.

To account for any remaining elastic signal not predicted by linearized ray theory, the companion technique to isolate the anelastic signal is the prediction and subtraction of the elastic signal using either the exact ray theoretic expressions of Woodhouse & Wong (1986) or the summation of coupled multiplets (Woodhouse 1980; Park & Gilbert 1986; Dahlen 1987; Park 1987) for the elastic earth model MPA12.4A of Wong (1989):

$$d_n^{\text{debias}} = d_n - d_n^{\text{pre}}(\oplus_{\text{el}}), \tag{4}$$

where $d_n^{\text{pre}}(\oplus_{\text{el}})$ is the datum predicted for the elastic reference model. The resulting datum is referred to as *debiased* relative to the input model of elastic structure. Any remaining elastic signal in the datum d_n^{debias} is attributable to errors in current long-period elastic models, effects of higher-degree elastic structure not predicted by linearized ray theory, and inaccuracies in forward theory. The results of the synthetic experiments in Section 4 will allow us to quantify these corrupting influences.

2.2 Iterative inverse problem

The general linearized relation between the desensitized data and model perturbations is represented by

$$d_n^{\text{obs}}(\omega) = d_n^{\text{pre}}(\omega, \oplus_{\text{el}}, \oplus_{\text{anel}}) + \frac{\partial d_n}{\partial c}\delta c(\omega) + \frac{\partial d_n}{\partial q}\delta q(\omega), \tag{5}$$

where c is the elastic phase velocity of the wave, q is the inverse quality factor, analogous to an imaginary part of phase velocity, and d^{pre} is the predicted anomaly for the earth model $\oplus$ which contains perturbations in elastic and anelastic structure. In this study, the elastic phase velocity, when used, is assumed fixed and known while the anelastic structure is iteratively perturbed, removing the perturbation term for elasticity in eq. (5),

$$\begin{aligned}\delta d_n(\omega)_i &= d_n^{\text{obs}}(\omega) - d_n^{\text{pre}}[\omega, c(\omega), q(\omega) + \delta q_i(\omega)] \\ &= \frac{\partial d_n}{\partial q}\delta q_{i+1}(\omega),\end{aligned} \tag{6}$$

where d_n^{pre} is, again, non-linearly related to the phase-velocity c and attenuation q. The *debiased* datum is equivalent to the first iteration of eq. (6), where the only aspherical signal in d^{pre} originates from the reference elastic model.

2.3 Partial derivative matrix

We have constructed an estimator which is dominantly sensitive to anelastic structure and in this section relate this observable to attenuation model parameters. The partial derivative matrix is calculated using results from geometrical ray theory, and is the anelastic counterpart to the location parameter formalism of Jordan (1978).

The amplitude anomaly attributable to anelastic structure may be represented by an exponential decay of the wave

$$a_n^{\text{anel}}(\omega) = \mathrm{e}^{-\delta\alpha(\mathbf{x},t,\omega)}, \tag{7}$$

where the perturbation in α is accumulated along the true wavepath

$$\delta\alpha = \frac{-\omega}{2}\left[\int_{\text{ray}} q(\omega,\theta,\phi)\,dt(\theta,\phi) - q_0(\omega)\int_{\substack{\text{great}\\\text{circle}}} dt(\theta,\phi)\right], \tag{8}$$

where q_0 denotes the spherical reference value of the wave attenuation. Applying the geometrical optics approximation, where the ray path is reduced to the great-circle connecting source and receiver, eq. (8) becomes

$$\delta\alpha = \frac{-\omega a}{2}\left[\int_0^\Delta \frac{q_0 + \delta q(\theta,\phi)}{U_0 + \delta U(\theta,\phi)}\,d\Delta(\theta,\phi) - \frac{q_0}{U_0}\int_0^\Delta d\Delta(\theta,\phi)\right] \tag{9}$$

$$\simeq \frac{-\omega a}{2}\left[\int_0^\Delta \frac{q_0}{U_0}\left(1 + \frac{\delta q}{q_0} - \frac{\delta U}{U_0}\right)d\Delta(\theta,\phi) - \frac{q_0}{U_0}\int_0^\Delta d\Delta(\theta,\phi)\right] \tag{10}$$

or, to first order in δq,

$$\delta\alpha = \frac{-\omega a}{2U_0}\int_0^\Delta \delta q(\theta,\phi)\,d\Delta(\theta,\phi), \tag{11}$$

where U represents group velocity and a denotes the Earth's radius. The term involving the velocity variation ($\delta U/U_0$) is roughly an order of magnitude smaller than the relative perturbation in q and is neglected. This expression may be written more generally as a path average

$$\delta\alpha = \frac{-\omega a}{2U_0}\Delta\langle\delta q(\omega)\rangle. \tag{12}$$

In the geometrical optics approximation, anomalies from consecutive wavepacket arrivals are thus influenced by anelastic structure according to

$$a_{n+2}^{\text{obs}}(\omega) = a_n^{\text{obs}}(\omega)\exp\left[\frac{-\omega a}{2U_0}2\pi\langle\delta q(\omega)\rangle\right], \tag{13}$$

where the perturbation in q is averaged over the great circle defined by the source and receiver.

The observable that may be attributed to anelastic structure only is given by

$$d_n^{\text{desen}}(\omega) = \left[\frac{a_{n+2}(\omega)}{a_n(\omega)}\frac{a_{n+3}(\omega)}{a_{n+1}(\omega)}\right]^{1/2} = \exp\left[\frac{-\omega a}{2U_0}2\pi\langle\delta q_n(\omega)\rangle\right], \tag{14}$$

or,

$$\left(\frac{-U_0}{\pi\omega a}\right)\ln\left(d_n^{\text{desen}}\right)=\left(\frac{-U_0}{\pi\omega a}\right)\ln\left[\frac{a_{n+2}(\omega)}{a_n(\omega)}\frac{\tilde{a_{n+3}}(\omega)}{a_{n+1}(\omega)}\right]^{1/2}$$
$$=\langle\delta q_n(\omega)\rangle, \tag{15}$$

and is insensitive to elastic structure according to linearized ray theory as well as being independent of source and instrument errors. The solution of the linear problem posed in eq. (15) constitutes the zeroth iteration in the iterative inversion for variations in surface wave attenuation.

The elements of the partial derivative matrix in eq. (6) are constructed from eq. (15) in which the path-averaged model perturbation $\langle\delta q(\omega)\rangle$ is replaced with an averaging integral along the great circle,

$$\langle\delta q(\omega)\rangle=\frac{1}{2\pi}\oint_{(\Theta,\Phi)}\delta q(\omega,\theta,\phi)\,ds \tag{16}$$

where (Θ,Φ) is the pole of the great circle defined by the source-receiver pair. The local perturbation $\delta q(\omega,\theta,\phi)$ is expanded in complex spherical harmonics following the convention of Edmonds (1960) and the expression for the path-averaged perturbation becomes

$$\langle\delta q(\phi)\rangle=\sum_{s,t}\delta q_s^t(\omega)\frac{1}{2\pi}\int_{(\Theta,\Phi)}Y_s^t(\theta,\phi)\,ds. \tag{17}$$

As shown by Backus (1964), the great circle average of spherical harmonics is expressible in terms of their value at the great circle pole:

$$\frac{1}{2\pi}\int_{(\Theta,\Phi)}Y_s^t(\theta,\phi)\,ds=\frac{P_s(0)}{P_s(1)}Y_s^t(\Theta,\Phi) \tag{18}$$

where P_s is the Legendre polynomial. Because the great circle average of odd harmonics vanishes, the geometrical optics approximation has restricted the solution space to even-degree structure, or structure which is symmetric under reflection through the Earth's centre.

The linear system for the lateral perturbations in surface wave attenuation becomes

$$\langle\delta q_n(\omega)\rangle_i=\sum_{s,t}\frac{P_s(0)}{P_s(1)}Y_s^t(\Theta_i,\Phi_i)\,\delta q_s^t(\omega), \tag{19}$$

where i denotes each source-receiver pair. The partial derivative matrix in eq. (6) is constant at each iteration; the relationship between the observed anomalies and model perturbations is linear in the geometrical optics limit. However, the predicted anomalies are non-linearly related to earth structure, requiring iteration to the solution. The accuracy of the iterative technique is dictated by the ability to predict the anomalies, which is done using accurate forward theory, and not in the accuracy of the partial derivative matrix, which here is only approximate. The validity of the partial derivative matrix does, however, influence the convergence properties of the system.

2.4 Inverse theory

For this overdetermined system, we seek to minimize the sum of the norm of the residual vector and the norm of the model vector

$$\min\left(\mathbf{d}^{\mathrm{T}}\mathbf{C}_{\mathrm{d}}^{-1}\mathbf{d}+\mathbf{q}^{\mathrm{T}}\mathbf{C}_{\mathrm{m}}^{-1}\mathbf{q}\right), \tag{20}$$

where $\mathbf{C}_{\mathrm{d}}$ is the data covariance matrix, incorporating errors in the data and $\mathbf{C}_{\mathrm{m}}$ is the model covariance matrix, incorporating *a priori* constraints on the solution [Jackson 1979: Tarantola & Valette 1982].

At each iteration, the model vector is given by

$$\mathbf{q}_{i+1}=\mathbf{q}_i+(\mathbf{A}^{\mathrm{T}}\mathbf{C}_{\mathrm{d}}^{-1}\mathbf{A}+\mathbf{C}_{\mathrm{m}}^{-1})^{-1}(\mathbf{A}^{\mathrm{T}}\mathbf{C}_{\mathrm{d}}^{-1}\mathbf{d}_i-\mathbf{C}_{\mathrm{m}}^{-1}\mathbf{q}_i), \tag{21}$$

where $\mathbf{d}_i$ is the residual signal after the signal from the fixed elastic model and current anelastic model $\mathbf{q}_i$ have been removed.

The resolving ability of the system is given by the resolution matrix (Backus & Gilbert 1967, 1968)

$$\mathbf{R}=(\mathbf{A}^{\mathrm{T}}\mathbf{C}_{\mathrm{d}}^{-1}\mathbf{A}+\mathbf{C}_{\mathrm{m}}^{-1})(\mathbf{A}^{\mathrm{T}}\mathbf{C}_{\mathrm{d}}^{-1}\mathbf{A}), \tag{22}$$

while the *a posteriori* covariance of the solution is given by

$$\mathbf{C}=\hat{\sigma}^2(\mathbf{A}^{\mathrm{T}}\mathbf{C}_{\mathrm{d}}^{-1}\mathbf{A}+\mathbf{C}_{\mathrm{m}}^{-1})^{-1}\mathbf{A}^{\mathrm{T}}\mathbf{A}(\mathbf{A}^{\mathrm{T}}\mathbf{C}_{\mathrm{d}}^{-1}\mathbf{A}+\mathbf{C}_{\mathrm{m}}^{-1})^{-1}, \tag{23}$$

where for N data, the *a posteriori* data variance is given by (Gubbins & Bloxham 1985)

$$\hat{\sigma}^2=\frac{\mathbf{d}^{\mathrm{T}}\mathbf{C}_{\mathrm{d}}^{-1}\mathbf{d}}{N-tr(\mathbf{R})}. \tag{24}$$

The information density matrix

$$\mathbf{D}=\mathbf{A}(\mathbf{A}^{\mathrm{T}}\mathbf{C}_{\mathrm{d}}^{-1}\mathbf{A}+\mathbf{C}_{\mathrm{m}}^{-1})\mathbf{A}^{\mathrm{T}}\mathbf{C}_{\mathrm{d}}^{-1} \tag{25}$$

measures the contribution of each datum to the final solution. The least-squares solution is inherently sensitive to outliers, a shortcoming which can be detected by the information density matrix.

The prior model covariance matrix $\mathbf{C}_{\mathrm{m}}$ is commonly taken to be a diagonal matrix of elements $\lambda\mathbf{C}_{\mathrm{d}}^{-1}$, where λ is a damping parameter restricting the solution from poorly resolved regions of solution space. Under this formulation, the solution is assumed to be normally distributed. The choice of λ should optimally strike a balance between resolution and error. The use of *a priori* weighting schemes on the data is reflected in the data covariance matrix $\mathbf{C}_{\mathrm{d}}$, since weighting reflects an assessment of data quality or accuracy.

3 DATA SELECTION

The data used in this study were extracted from long-period three-component seismograms recorded by the Global Digital Seismic Network (GDSN) and vertical component records from the International Deployment of Accelerometers (IDA). Amplitude anomalies were measured from 1610 vertical, 790 longitudinal and 1140 transverse seismograms associated with 144 events between 1978 and 1984. Since anomalies from four consecutive surface wave orbits are required in the inversion, the number of available data is reduced to 1339 desensitized observations for Rayleigh waves with 374 reduced data from orbits R_1–R_4, 609 from R_2–R_5, 267 from R_3–R_6, 82 from R_4–R_7, and 7 R_5–R_8. While the R_1 arrival from large events ($M_s>6.5$) can saturate the GDSN instruments, we were able to extract several hundred observations of R_1 from smaller events. Fig. 3 presents the distribution of events and the poles of the great circle paths used to study Rayleigh wave attenuation.

To measure the surface wave amplitude anomalies, the data are referenced to a synthetic seismogram constructed

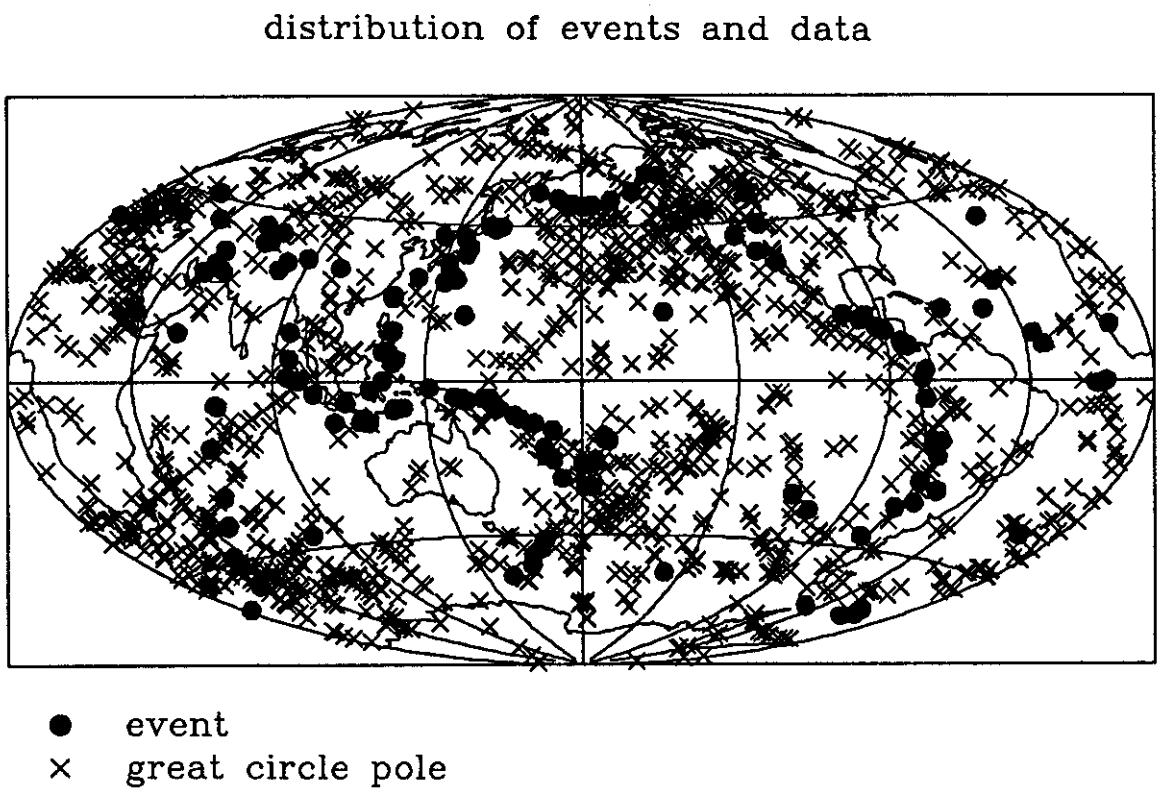

Figure 3. Distrubtion of 144 events and great-circle pole position of each source-receiver pair used in this study.

for the spherical reference earth model PREM (Dziewonski & Anderson 1981) and source parameters provided by the Centroid Moment Tensor (CMT) catalogue (Dziewonski, Chou & Woodhouse 1981). For each surface wave orbit, a 30 min time window is applied, centred at the arrival corresponding to the group velocities $3.6\,\mathrm{km\,s^{-1}}$ and $4.4\,\mathrm{km\,s^{-1}}$ for Rayleigh and Love waves, respectively. For each extracted wavepacket, the amplitude and phase anomalies are determined from the transfer function which maps the synthetic reference spectra to the observed spectra

$$\bar{u}_{\mathrm{sph}}(\omega) \cdot A(\omega) e^{i\psi(\omega)} = \bar{u}_{\mathrm{obs}}(\omega), \tag{26}$$

where $\bar{u}_{\mathrm{sph}}(\omega)$, $\bar{u}_{\mathrm{obs}}(\omega)$ are the Fourier transforms of the synthetic and observed wavepackets, respectively. The amplitude and phase transfer functions are parameterized by a quadratic function of frequency and the polynomial coefficients are determined by non-linear least squares, yielding the transfer functions $[A(\omega), \psi(\omega)]$ over the period range of 150–270 s. In the period range of 270–300 s, it is sufficient to parameterize the transfer function as linear. For further discussion on the formation of the transfer function, the reader is referred to Wong (1989). The advantage of expressing the transfer function as a smooth function of frequency is that it minimizes the effects of spectral noise from data truncation and unwanted signal, such as overtones.

The editing criterion requires an adequate signal-to-noise ratio and relative isolation of the wave packets; receivers near the antipode are rejected due to interference of even and odd orbiting wavepackets. Furthermore, observations from deep events (>80 km) are rejected to reduce overtone interference.

4 SYNTHETIC EXPERIMENTS

The ability to accurately and efficiently calculate surface wave amplitude and phase anomalies for specified earth structure exists, either using fully coupled normal mode theory (Park 1987) or surface wave ray theory (Woodhouse 1974; Jobert & Jobert 1983; Woodhouse & Wong 1986), allowing a synthetic data set to be generated and the properties of the estimator investigated. In this section, we perform synthetic experiments designed to illuminate two aspects of the inversion for surface wave attenuation. First, we attempt to quantify the consequences of the inability to completely isolate the anelastic signal from elastic contamination. Second, we confirm that the approximate partial derivative matrix used allows convergence to the input anelastic model.

Unless otherwise stated, for each experiment two synthetically generated data sets are constructed and investigated; one using fully coupled normal-mode theory and the other using the ray-theoretic formalism. The normal-mode synthetics comprise the spheroidal modes from ${}_0S_{15}$ to ${}_0S_{75}$ and include first-order coupling of each multiplet to its nearest 10 neighbours along the fundamental mode branch. The observations are obtained from the synthetic seismograms in the same manner as for the real data. For the ray theoretic predictions, the amplitude anomalies $a(\omega)$ are given directly by the theory.

The first three experiments examine the biasing effects of elastic structure and emphasize the need to eliminate the elastic signal from the observed anomalies. The synthetic data sets for these three experiments duplicate the observations in both distribution and number. The results

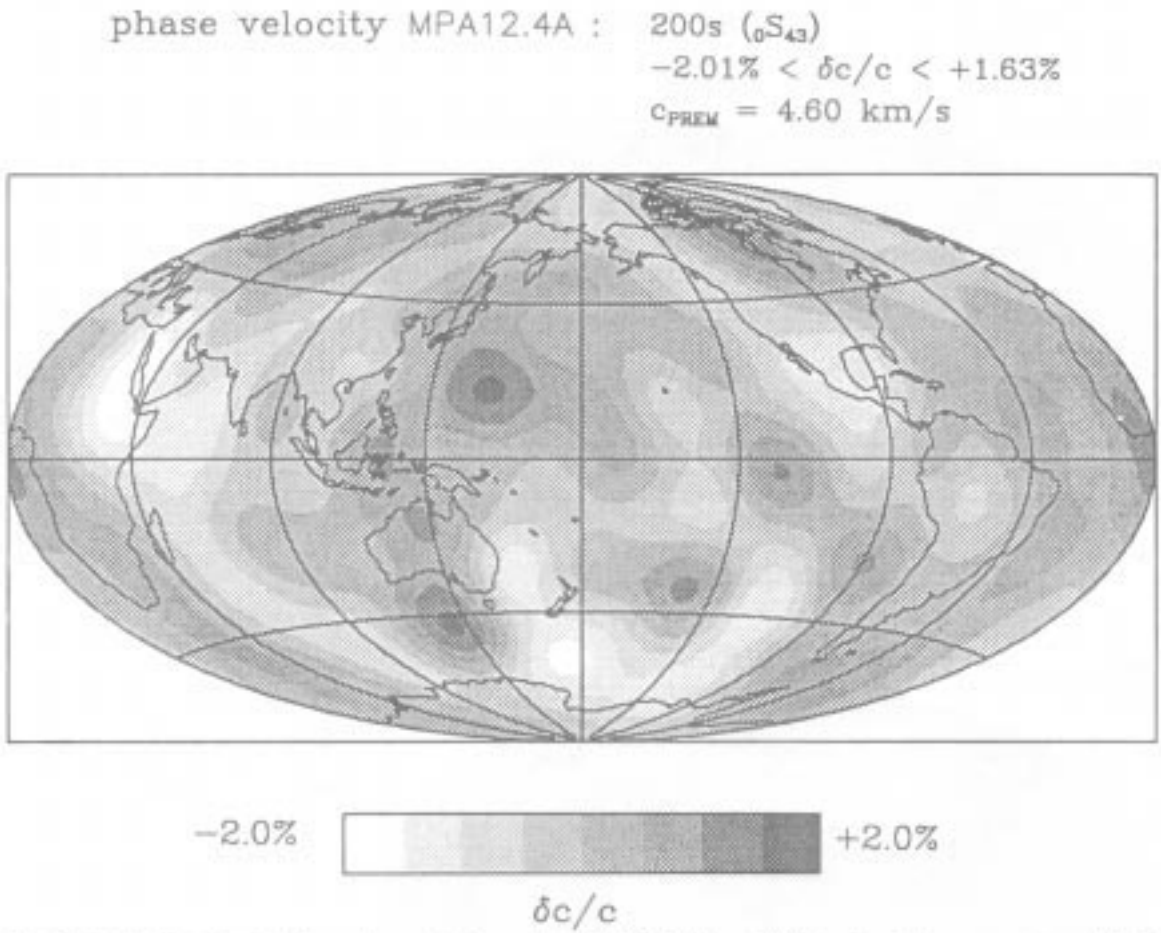

Figure 4. The phase velocity calculated from shear velocity model MPA12.4A (Wong 1989) for Rayleigh waves at a period of 200 s. Such elastic models are used to estimate the remaining elastic signal in the *desensitized* amplitude data.

are presented for Rayleigh waves with a 200 s period ($_0S_{43}$). The normal mode synthetics are calculated using a hybrid model: M84A (Woodhouse & Dziewonski 1984) for spherical harmonic degrees 1–8 and MPA12.4A (Wong 1989) for degrees 9–12 and hereinafter referred to as M84.12A. For the ray theoretic predictions, the elastic input model is MPA12.4A (Fig. 4). The difference in the use of the elastic models is merely historic. Because the phase velocity is depth averaged, the differences between the two models are found to affect the predicted amplitude anomalies insignificantly for a given forward technique and the models may be considered equivalent.

The fourth and final experiment considers the retrieval of an input model of surface wave attenuation, demonstrating the convergence properties of the iterative method. In contrast to the first three experiments, the synthetic data set is constructed for 25 geographically well distributed events and 700 source-receiver pairs and the data set only consists of normal mode synthetics which consider multiplet self coupling through elastic and anelastic structure. The anelastic model is chosen to possess a degree 12 zonal structure with a realistic variation in the quality factor q of roughly ±40 per cent (Fig. 8a). While unrealistic in geometry, such a choice facilitates an easy observational assessment of the convergence of the iterative technique (eq. 6).

Results of synthetic experiments

The basic characteristics of each experiment, nos. 1–4, are presented in Table 1. In the following we discuss the motivation for, and results of, each synthetic experiment.

Experiment no. 1: apparent attenuation: no desensitization

This experiment demonstrates the consequences of adopting amplitude anomalies as a measure of wave attenuation. The

Table 1. The characteristics of the four synthetic experiments. Experiments nos. 1–3 aim to determine the magnitude of elastic bias due to elastic focusing effects while experiment no. 4 investigates the convergence properties of the iterative inversion. The elastic input model used in constructing the synthetic data in each case is M84.12A, or some component of it. The use of an elastic reference model corresponds to the first iteration of the inversion; in the absence of an elastic reference model the number of iterations is zero.

Experiment Characteristic	Exp #1	Exp #2	Exp #3	Exp #4
Elastic Input Model ?	M84.12A	M84.12A	M84.12A(s=0.12)	M84.12A
Anelastic Input Model ?	No	No	No	Yes
Desensitization ?	No	Yes	Yes	Yes
Elastic Reference Model ?	No	No	M84.12A(s=0.10)	Yes
Number of Iterations	0	0	1	3

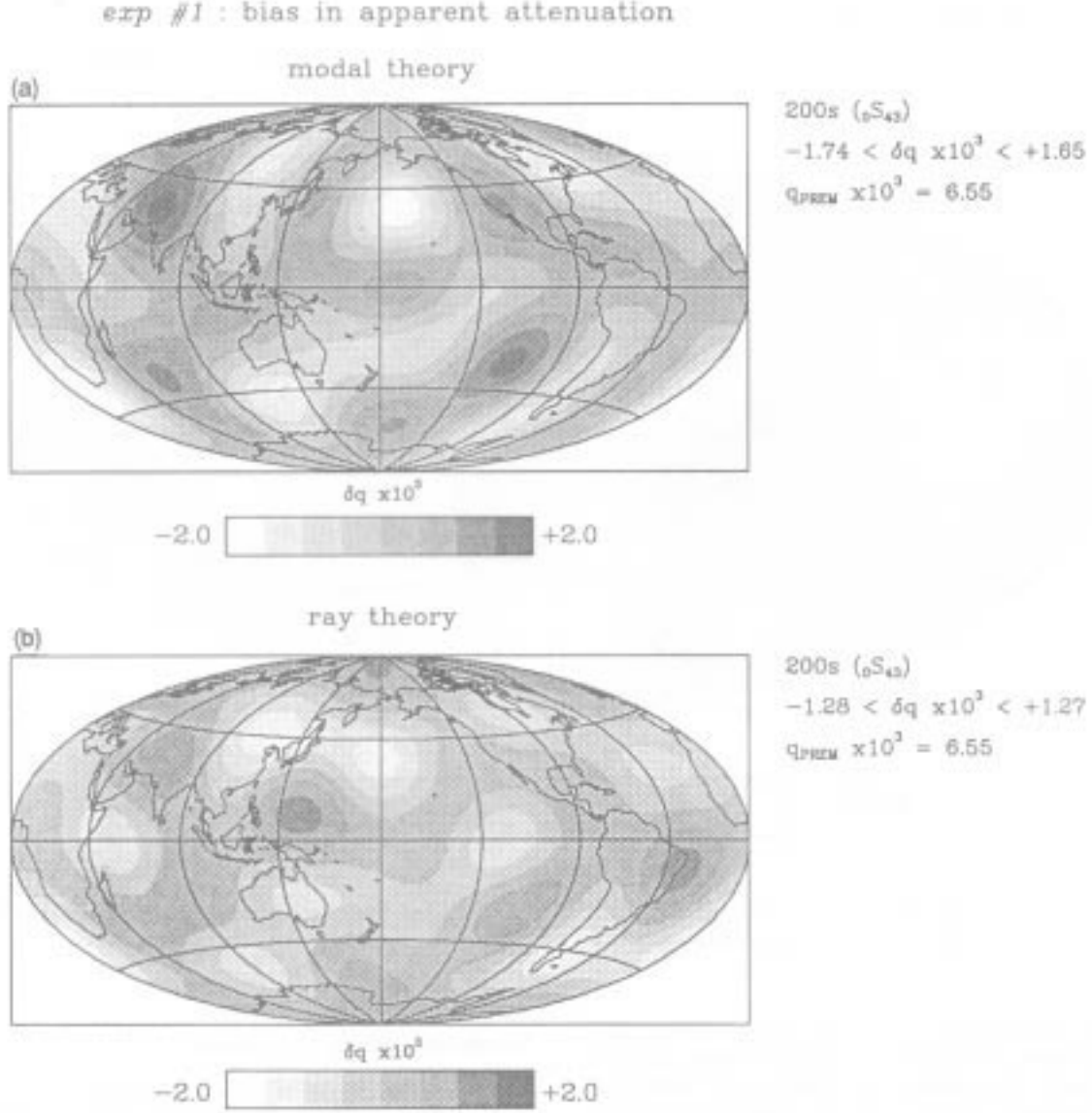

Figure 5. *Synthetic experiment no. 1:* in synthetic experiments nos. 1–3, the signal in the synthetic data set is from aspherical elastic structure and spherical anelastic structure while the number and distribution of the synthetic data set duplicate those of the real data. This figure shows apparent attenuation retrieved when no attempt has been made to reduce the elastic signal, demonstrating the considerable bias which elastic structure may induce.

only aspherical signal in the synthetic data is from the input elastic model; there is no input aspherical Q or noise. The data are inverted as though all anomalous signal is attributable to anelasticity; no attempt is made to reduce the elastic signal. Results are displayed with attenuation maps at a given frequency where:

$$\delta q(\omega, \theta, \phi) = \sum_{s,t} \delta q'_s(\omega) Y^t_s(\theta, \phi). \tag{27}$$

The retrieved attenuation maps for synthetic data constructed using normal-mode summation (Fig. 5a) and asymptotic ray theory (Fig. 5b) reveal 30 per cent variations in Q^{-1} even though the input anelastic model is spherical. This example demonstrates that amplitudes alone are a poor measure of attenuation and quantifies the bias when elastic focusing is completely ignored.

Experiment no. 2: bias in zeroth iteration: desensitization

In experiment no. 2, we test the effectiveness of desensitizing the data to remove the elastic signal as described in Section 2. The conditions of the previous experiment are duplicated except that in this experiment, the synthetic data are *desensitized* to elastic structure, as suggested by linearized ray theory [eq. (3)]. The information in the synthetic data remains unchanged, consisting of spherical anelasticity, aspherical elasticity, and no noise. If data desensitization is successful in isolating the anelastic signal, the retrieved attenuation model should be the null model. The retrieved attenuation models (Figs 6a and 6b) demonstrate that desensitization has removed roughly two-thirds of the elastic bias compared to the inversion of raw-amplitude anomalies, but significant elastic signal

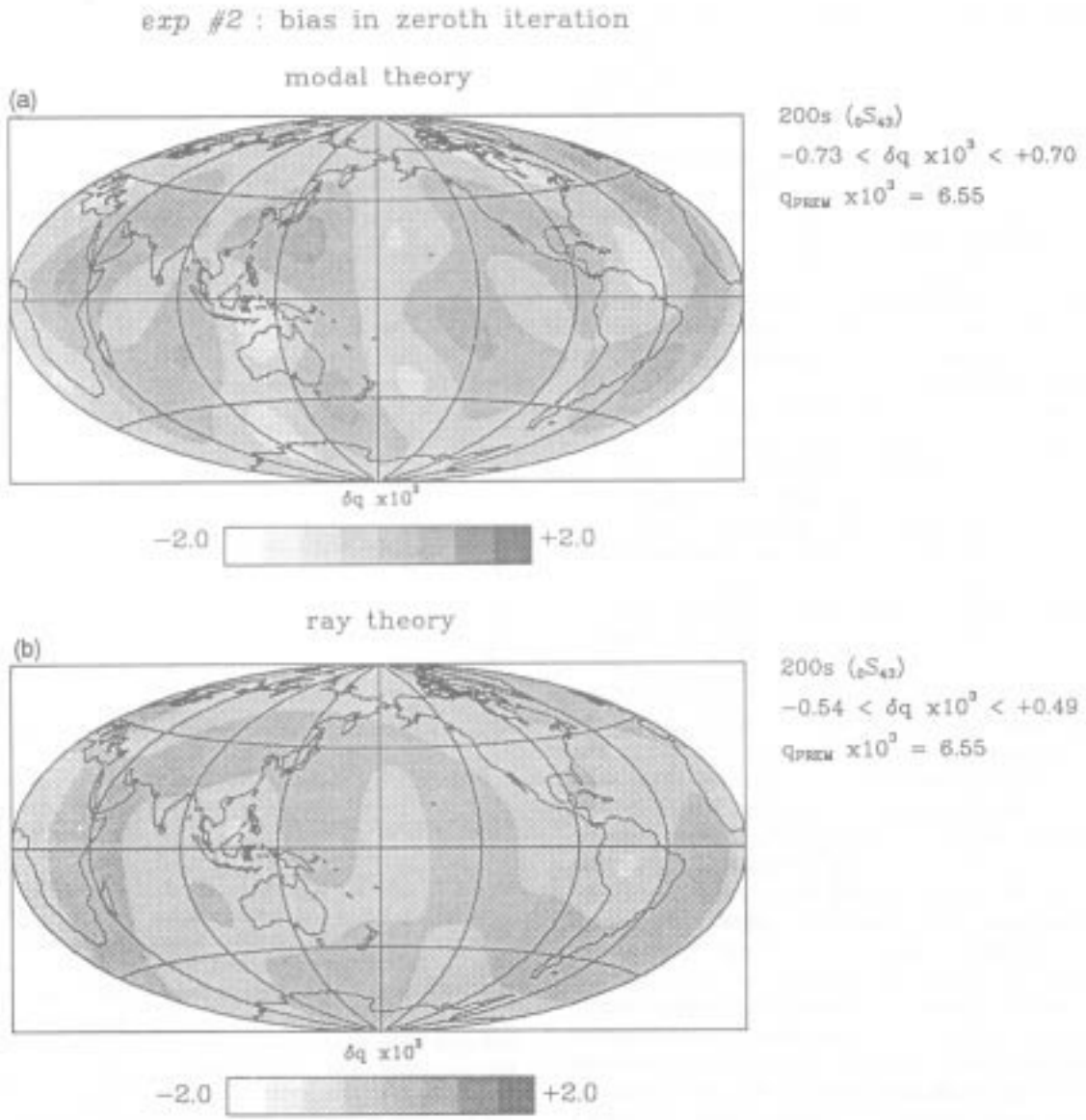

Figure 6. *Synthetic experiment no. 2:* the results of the zeroth iteration, where the synthetic amplitude anomalies are *desensitized* (see Section 2) to elastic structure as suggested by linearized ray theory. Elastic bias has been considerably reduced from *experiment no. 1*, but the magnitude of the bias is roughly 30 per cent of the models retrieved from real data. The synthetic data are constructed using (a) normal-mode summation and (b) full ray theory.

remains, presumably due to departures from linearized ray theory. The correct null attenuation model does not lie within one standard deviation of the retrieved models. The elastic bias is roughly 10 per cent of q_{PREM} and 30 per cent of the anelastic models retrieved from data, presented in the next section. While successful in reducing elastic signal, desensitization is insufficient when applied alone.

It should be pointed out that the mapping of elastic signal into retrieved anelastic models is not random, but is systematic and reproducible for any subset of the data that similarly samples the earth. Thus, breaking the data set in half and demonstrating the similarity of retrieved structures does not establish the believability and accuracy of the models.

To reduce this elastic bias further necessitates the use of an existing aspherical elastic model as a reference model in eq. (6). Thus, although desensitizing the data reduces the effects of elastic focusing and defocusing in a way that requires no *a priori* knowledge of elastic structure, the remaining elastic bias caused by departures from linearized ray theory must be removed by introducing more information into the estimator through the introduction of an elastic reference model.

Experiment no. 3: bias from short-wavelength elastic structure

In this synthetic experiment, we attempt to quantify the effect of shorter wavelength elastic structure on long-wavelength retrieved anelastic structure. The synthetic data set contains signal from the degree 12 elastic model MPA12.4A, no aspherical anelastic structure, and no noise.

The synthetic data set is generated using exact ray theory. We desensitize the data and debias it by predicting and removing the elastic signal using a slightly incorrect model; in this case, degrees $s = 0$–10 of the input elastic model. We test the ability of the remaining degree 11 and 12 elastic signal to bias retrieved long-wavelength attenuation models. In this sense, the remaining elastic signal is treated as though originating from unknown short wavelength elastic structure. Ultimately, the experiment would be more realistic if an aspherical elastic model with structure well beyond degree 12 was incorporated. However, the results of this experiment allow us to estimate roughly the extent to which elastic structure at one wavelength maps into retrieved attenuation models.

Because phase anomalies are linearly related to velocity anomalies, the absence of the degree 11 and 12 structure does not greatly affect phase anomaly predictions and the incorrect model still explains 91 per cent of the variance. For amplitude anomalies, which are also sensitive to the gradients of the velocity anomalies, the absence of the short-wavelength structure leads to greater error in the predicted values, with a variance reduction of 63 per cent for the amplitude anomalies and 54 per cent for the desensitized data.

Fig. 7(a) presents the maximum deviation of the retrieved attenuation model as a percentage of PREM where the regression has been performed for degrees 2, 4 and 6. The attempt to debias the data using an elastic model that lacks the short-wavelength structure of the input model reduces the bias by half on average. In Fig. 7(b), the regression is extended to degree 12 and the remaining elastic bias decreases as the wavelength of the retrieved anelastic structure increases. This behaviour suggests that elastic structure dominantly maps into anelastic structure of approximately the same wavelength. We are currently unable to estimate exactly the effects of all higher-degree elastic structure on the retrieved models; the elastic signals from the higher degrees may constructively or destructively interfere with the details depending on the exact nature of higher-degree elastic structure. However, since the earth's spectrum of heterogeneity is relatively enriched in longer-wavelength structure, the largest problem will probably result from bias due to the longest wavelengths, much of which is eliminated by the elastic reference model. Nevertheless, we feel that the problem of potential higher-degree elastic bias merits further investigation.

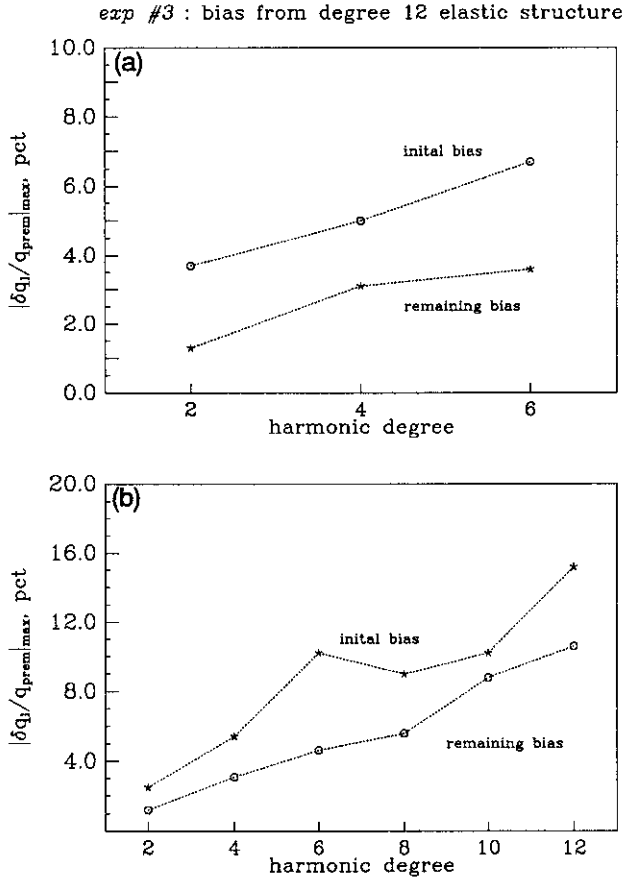

Figure 7. *Synthetic experiment no. 3:* the predicted mapping of signal from short-wavelength elastic structure into retrieved anelastic structure. The synthetic densensitized data are constructed from the degree 12 model MPA12.4A. The data are debiased using only the degree 0–10 components of the input model. The remaining elastic signal is treated as though originating from unknown short-wavelength elastic structure. The bias is defined as the maximum value of $|\delta_q(\theta, \phi)/q_{\mathrm{PREM}}|$ at each degree of the expansion. In (a) the synthetic data have been inverted exactly as the real data with a degree 6 expansion for lateral variations in surface wave attenuation while in (b), the expansion was extended to degree 12.

Experiment no. 4: retrieval of anelasticity

In addition to elastic structure, the synthetic data here contain signal from an even-degree, zonal aspherical anelastic model at degrees $s = 2$, 4, 6, 8, 10, 12 that possesses a half-peak-to-peak variation in q of roughly 40 per cent of q_{PREM}. The moduli of the input complex q_s^0 coefficients as well as the estimated coefficients for the first three iterations of eq. (6) are given in Table 2. Table 2 also lists the retrieved attenuation coefficients when raw-amplitude anomalies are used and when anomalies are desensitized but no reference elastic model is employed (iteration 0). In addition, Table 2 lists the root-sum-modulus squared of the retrieved non-axisymmetric coefficients $|q_s^t|_{t\neq 0}$:

$$|q_s^t|_{t\neq 0} = \left[\sum_{t=1}^{s} (|q_s^t|^2 + |q_s^{-t}|^2)\right]^{1/2}, \tag{28}$$

where $|q| = (q^* q)^{1/2}$ and * denotes complex conjugation. The estimated attenuation maps are displayed in Fig. 8. Because the synthetic data contain no noise, undamped inversions were performed. Convergence is observed toward the input coefficients and it is obvious that the unmodelled anelastic signal from short wavelength structure above degree 6 is only weakly influencing the retrieved attenuation coefficients. When damping similar to that used in the data inversions was applied to the perfect synthetic data, the input model was underpredicted by roughly 30 per cent. While this procedure is incorrect since none of the synthetic data variance is due to noise, it provides an upper bound on the effect of damping on the retrieved model size.

We have confirmed that the ability to converge to the

Table 2. *Synthetic experiment no. 4:* comparison of the input attenuation coefficients with the retrieved coefficients at each iteration. The input attenuation is a degree 12 zonal model. The zonal term ($m = 0$) is compared to the length of the non-zonal terms for each degree. The shortest wavelength attenuation structure in the input model does not significantly bias the retrieved model.

	degree 2		degree 4		degree 6	
	$\delta q_s^0 \times 10^3$	$\lvert\delta q_s^t\rvert_{t\neq 0} \times 10^3$	$\delta q_s^0 \times 10^3$	$\lvert\delta q_s^t\rvert_{t\neq 0} \times 10^3$	$\delta q_s^0 \times 10^3$	$\lvert\delta q_s^t\rvert_{t\neq 0} \times 10^3$
input model	2.1020	0.0000	0.6961	0.0000	2.1893	0.0000
apparent atten	1.5290	0.9519	1.0725	1.2455	2.5177	1.9619
iteration 0: *desen*	1.8791	0.7457	1.0123	0.9960	2.8677	1.2177
iteration 1: *debias*	1.9513	0.0589	0.5487	0.0783	1.9082	0.1753
iteration 2	2.1030	0.0024	0.6754	0.0508	2.1541	0.0483
iteration 3	2.0996	0.0020	0.6849	0.0449	2.1923	0.0429

correct solution depends on the ability to predict accurately the data residual and not on the accuracy of the geometrical optics approximations used to calculate the partial derivative matrix. Thus, the errors in the final models of attenuation are not a function of the errors in the partial derivative matrix. However, the computational ease of the geometrical optics approximations comes at the sacrifice of restricting us to consider only even-degree structure.

The synthetic experiments in this section have demonstrated the convergence of the iterative algorithm defined by eq. (6), emphasized the necessity of properly treating the elastic signal, and have helped quantify potential bias due to unmodelled signal. In applications to data, departures of the estimator from the true attenuation structure are a result of our inability to eliminate the influence of elastic and short wavelength anelastic signal perfectly. Desensitization is most accurate in reducing the data sensitivity to the long-wavelength elastic structure and the elastic reference model does not model the elastic bias caused by structure above degree 12. We believe that the most likely cause of remaining bias in the data is due to short-wavelength elastic structure.

5 RETRIEVED SURFACE WAVE ATTENUATION MAPS

In this section, the isolation of anelastic signal and inversion for lateral variations in surface wave attenuation, as presented in Section 2, are applied to the data described in Section 3. In the inversion, the heterogeneous attenuation is described by a truncated spherical harmonic expansion of degree 6 yielding a total number of parameters of 28. The damping is chosen to achieve a small magnitude model which explains most of the data, restricting unjustified small-scale structure. The damping values used allow roughly 21 degrees of freedom as determined by the trace of the resolution matrix. Because of the damping philosophy, which tends towards the smallest model which explains the majority of the data, the retrieved models may be considered lower bounds on acceptable model sizes. From experimentation, the geographical distribution of the heterogeneity is a robust feature that varies little with damping. Further, the geometry and, to a lesser extent, the size of the model through degree 6, is found to change insignificantly as the truncation of the expansion is increased beyond degree 6. However, the variance reduction afforded by the additional structure is insufficient to justify the additional degrees of freedom.

Observations from higher orbit arrivals are subject to increased contamination due to the reduced validity of linearized ray theory as well as an inherently smaller signal-to-noise ratio. Initially, an exponentially decaying weight is applied to reduce the dependence of the retrieved models on information from higher orbit arrivals. The residual variances for data from each orbit are then calculated *a posteriori* and the inversion is reperformed incorporating the *a posteriori* variances as weights, or measures of error for each class of data. The intention is to approach uniform data variance which is required for the least-squares solution to coincide with the maximum likelihood solution.

Fig. 9 presents the even-degree surface wave attenuation maps obtained for Rayleigh waves at 240, 200 and 160 seconds (${}_0S_{34}$, ${}_0S_{43}$, ${}_0S_{57}$). These results are for the zeroth iteration, where the data have been *desensitized* according to linearized ray theory. The models are for perturbations in Rayleigh-wave attenuation $\delta q(\omega, \theta, \phi)$ at a given frequency and are analogous to the elastic phase velocity of a wave in their depth averaging of, and linear relationship to, intrinsic structure. As the period decreases, the sensitivity of the surface waves to structure is compressed towards the surface. Fig. 10 demonstrates the sensitivity kernels of the Rayleigh waves to anelastic structure at the three periods shown in Fig. 9. If the elastic signal had been ignored and the inverted observations were biased-amplitude anomalies alone, the retrieved models would be roughly 50 per cent larger and have a significantly stronger zonal degree 2 feature, more closely resembling known elastic structure.

Figures 11 and 12 present the retrieved Rayleigh-wave attenuation after the first iteration, in which any remaining elastic signal due to departures in linearized ray theory has been estimated and removed. In Fig. 11, normal-mode calculations coupling the ten nearest neighbours to each

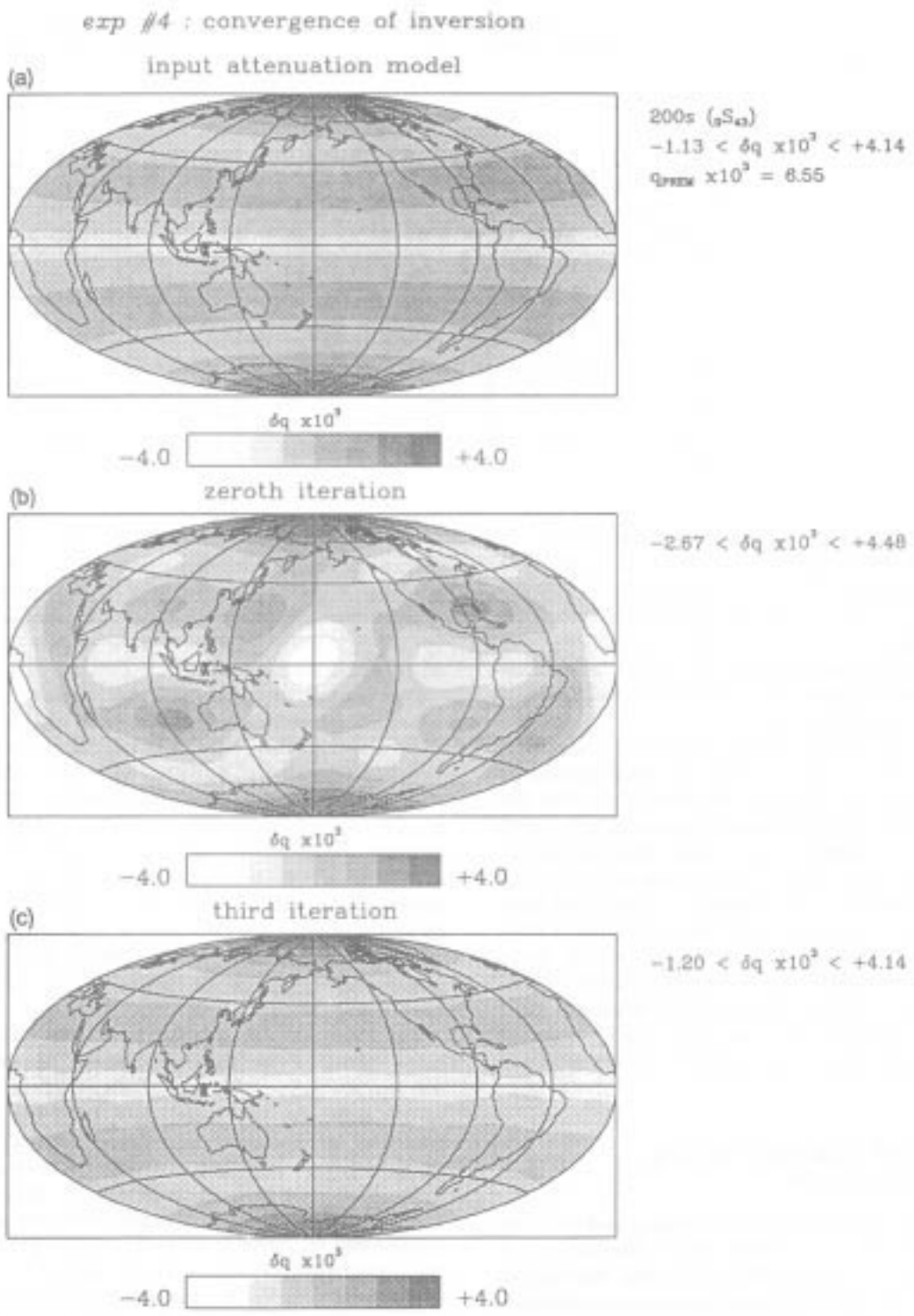

Figure 8. *Synthetic experiment no. 4:* retrieved anelasticity for synthetic data constructed using elastic model M84.12A (see text) and a zonal anelastic input model. (a) Degrees 2 through six of the even-degree 12 input anelastic model. (b) Retrieved attenuation after the zeroth iteration. (c) After the third iteration, the convergence to the input model is essentially complete.

multiplet were used to extract remaining elastic signal, while in Fig. 12, the elastic signal was predicted using expressions provided from exact surface wave ray theory.

Considering the geometry of the anelastic models for the two iterations, removal of the elastic signal through *debiasing* refines the view of anelasticity. When applying normal mode corrections, the geometry changes little but the model size is significantly perturbed, a result of the fact that the biased model predicted by modal theory is well correlated with the retrieved anelastic model (compare Figs 6a and 11b). Such a situation, where the false mapping obtained from elastic bias and the retrieved attenuation

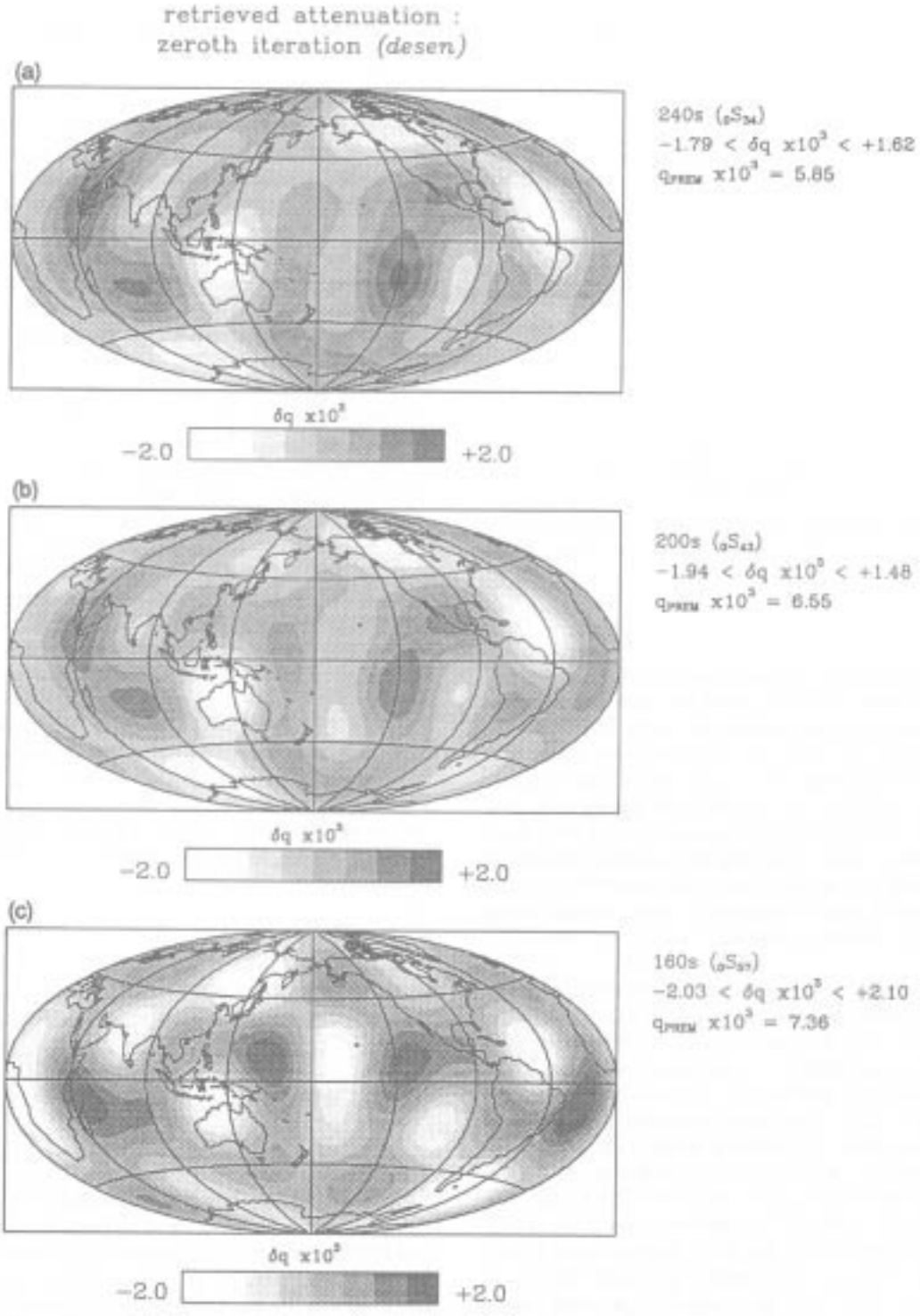

Figure 9. Retrieved perturbations in Raylegh-wave attenuation $\delta q(\theta, \phi, \omega)$ from observations of amplitude anomalies for Rayleigh waves at periods of (a) 240, (b) 200 and (c) 160 s. These results are for the zeroth iteration where the reduction of biasing elastic signal is accomplished by *desensitization* of the data according to linearized ray theory. The heterogeneity maps are analogous to phase velocity and sample the mantle identically.

model are correlated, emphasizes the need to address properly the presence of biasing elastic signal in the data. The application of ray theoretic corrections only slightly modifies the size and geometry of the retrieved models.

Fig. 13 presents the modulus of each degree of the attenuation models for the results of the first two iterations. The general trend is that the modulus decreases with decreasing period until 240 s at which point the model size increases with decreasing period. In the zeroth iteration, a slight decrease in degree 2 attenuation occurs until 180 s, suggesting either a slight signature of a deep degree 2 source of anelastic signal or a biased signature from the large

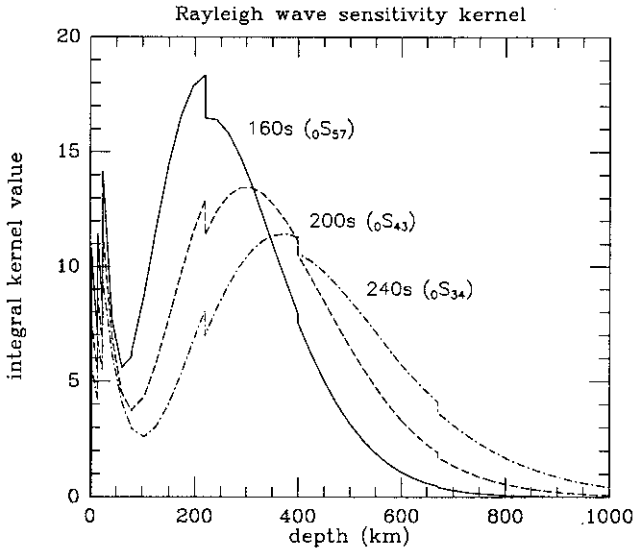

Figure 10. The integral kernels that govern the radial sensitivity of Rayleigh waves to Earth structure plotted for the same periods discussed in Fig. 9.

degree 2 elastic structure in the transition zone. In the first ieration, the models obtained when the data are debiased according to normal-mode predictions exhibit more extreme modification, with the model size decreasing by 30 per cent near 200 s and increasing by 50 per cent at the extreme ranges of interest. In the case in which ray theory is used to remove elastic bias, the attenuation models vary little from the zeroth iteration, where the data are only desensitized. In the first iteration, the degree 2 decrease observed after the zeroth iteration is either eliminated, using normal mode corrections, or slightly reduced, using ray theoretic corrections.

Fig. 14 is the relative variance for the retrieved anelastic models. In each plot, the upper curve is the relative variance in the debiased data attributable only to the removal of elastic signal as predicted by forward theory, while the lower curve is the variance attributable to both the elastic and anelastic models. The upper plot represents the results of applying normal-mode corrections while the lower plot considers ray theory. Modal theory provides an additional variance reduction of 10 per cent near 200 s, but has difficulty at shorter periods. Experiments have have shown that the edge effects due to the finite summation of modes has negligible effect on the ability of modal theory to improve the variance at high frequency. A more likely explanation for the difficulty at high frequency is that at this range, modes are more abundantly and strongly coupled and that the assumptions of first-order coupling and relative isolation of modes along the fundamental branch are less applicable. Ray theory has difficulty at low frequency but improves greatly with increasing frequency, as would be expected. The variance reduction has a maximum of 35 per cent near 150 s. Because d_n is a reduced datum, constructed from four consecutive amplitude anomalies, its accurate prediction may be more sensitive to approximations in the forward theory, leading to smaller variance reduction than might be expected.

6 SOURCE REGION OF ASPHERICAL ANELASTICITY

Qualitatively, the geometry of the surface wave attenuation maps (Fig. 12) are strikingly similar over a broad frequency range, suggesting that the source region of anelastic heterogeneity is similarly sampled by surface waves at the three periods. Referring to Fig. 10 which demonstrates the radial sensitivity of Rayleigh waves at the corresponding periods, we observe that the only region commonly sampled at all three periods is shallow, in or near the low velocity zone, defined as the region between 80–200 km depth.

The frequency dependence of the Rayleigh-wave attenuation maps, plotted in Fig. 13, demonstrates that as the sensitivity to shallow structure increases with increasing frequency, the modulus of the coefficients in all degrees generally increases. In contrast, the frequency dependence of the magnitude of the elastic phase velocity coefficients (Fig. 15) shows the strong degree 2 signal from the transition zone, manifested as a strongly decreasing magnitude in degree 2 structure with decreasing period. Because of the contrast in the power of the surface wave attenuation and phase velocity with frequency, even though the intrinsic structure is sampled identically, the dominant source region of anelastic heterogeneity must be different than that for elasticity and is likely to reside in the shallower mantle.

To gain a quantitative understanding of the 3-D intrinsic anelastic structure, we start with the plausible physical hypothesis that intrinsic elastic and anelastic heterogeneity are correlated at every depth. Since it is likely that attenuation variations are dominantly temperature controlled and radial derivatives of temperature are larger than lateral gradients, we confine ourselves to a radial-dependent proportionality coefficient

$$\alpha(r) = \frac{\delta q_u(r)}{\delta \ln v_s(r)}, \tag{29}$$

which maps intrinsic velocity into intrinsic anelasticity. The retrieved surface wave attenuation coefficients are linearly related to known intrinsic shear velocity perturbations, δv, by

$$\delta q_s^t(\omega_j) = \int_0^{R_\oplus} K_s(r, \omega_j)\left[\alpha(r)\frac{\delta v_s^t(r)}{v(r)}\right] r^2\, dr, \tag{30}$$

with $K(r, \omega_j)$ being the radial sensitivity kernel for the surface wave at frequency ω_j (Woodhouse & Dahlen 1978). Adopting the aspherical shear velocity model M84A for δv and PREM for v, eq. (30) forms a linear system to be solved for the proportionality profile, $\alpha(r)$. The conclusions from this inversion are not sensitive to the choice of the reference elastic model.

In the first inversion for the radially dependent proportionality coefficient $\alpha(r)$, the mantle is treated as a four-layer model, corresponding to the lid (0–80 km), the low-velocity zone (80–220 km), the high-gradient zone (220–400 km), and the transition zone (400–670 km), in which α is chosen to be constant in each layer. In the inversion, the proportionality coefficient is at all times required to be negative, based on the physical argument that realistic physical mechanisms for heterogeneity produce a velocity increase with a decrease in attenuation. The results of the inversion, in Fig. 16, reveal a proportionality constant

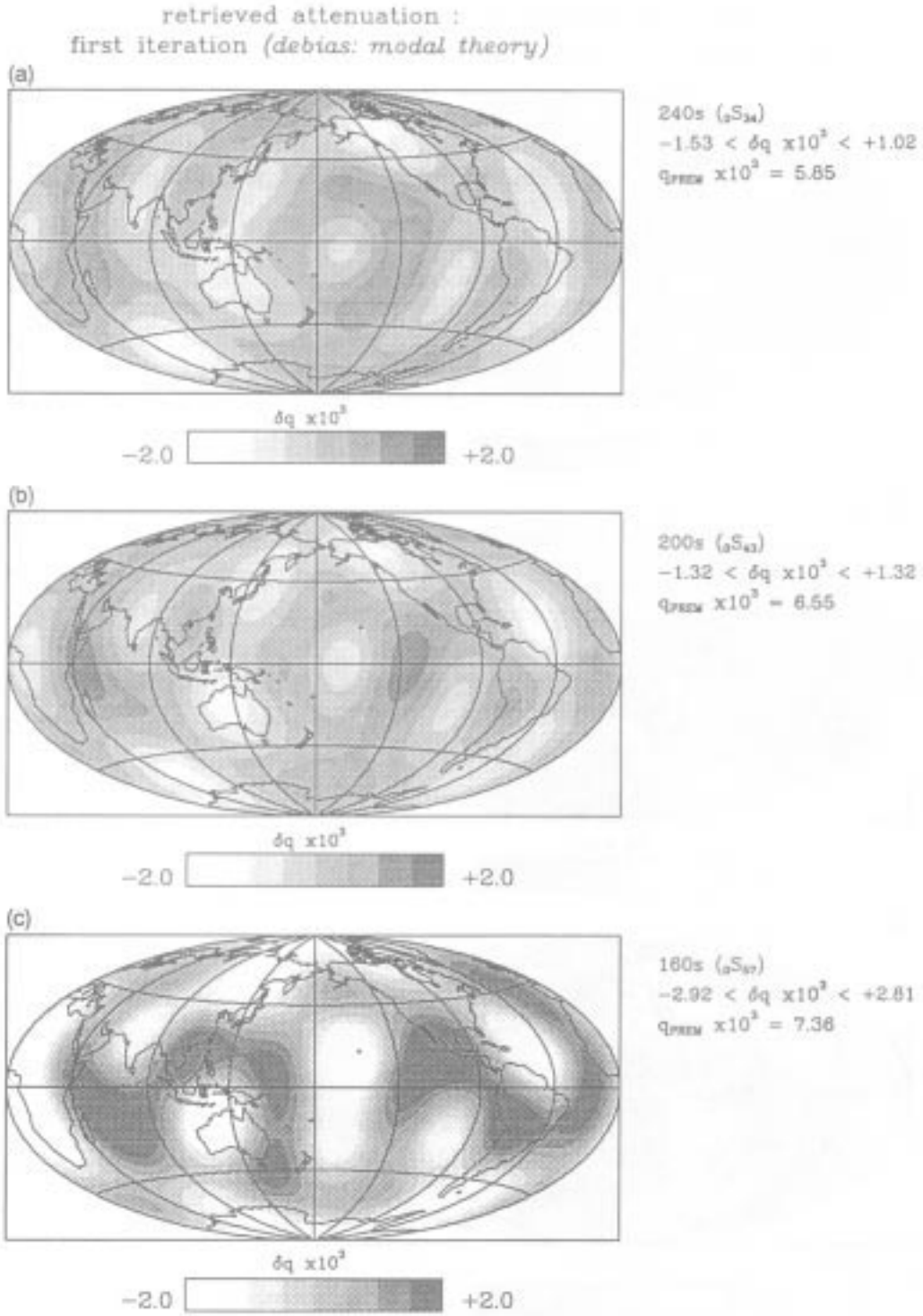

Figure 11. Retrieved Rayleigh wave attenuation $\delta q(\theta, \phi, \omega)$ after the first iteration in which the data have been *debiased*. The remaining elastic bias in the desensitized data has been estimated and removed using the known elastic model M84.12A (see text) and normal-mode calculations.

that is greater in the low-velocity zone and negligible in the upper mantle below 400 km. Fig. 16(a) presents the results using the attenuation coefficients from the zeroth iteration, using desensitized data, while in Figs 16(b) and 16(c), the attenuation coefficients from the first iteration are used, where the data are debiased according to normal-mode theory and ray theory, respectively. Inverting for the proportionality coefficients for individual degrees of the ray-theoretic model (Table 3) in Fig. 17 suggests that the degree 2 anelastic structure favours a component of $\alpha(r)$ in the deeper mantle while the source region for the degree 4 and 6 structures become increasingly shallow.

To further investigate the result that the structure in the shallow mantle alone can explain heterogeneous anelastic

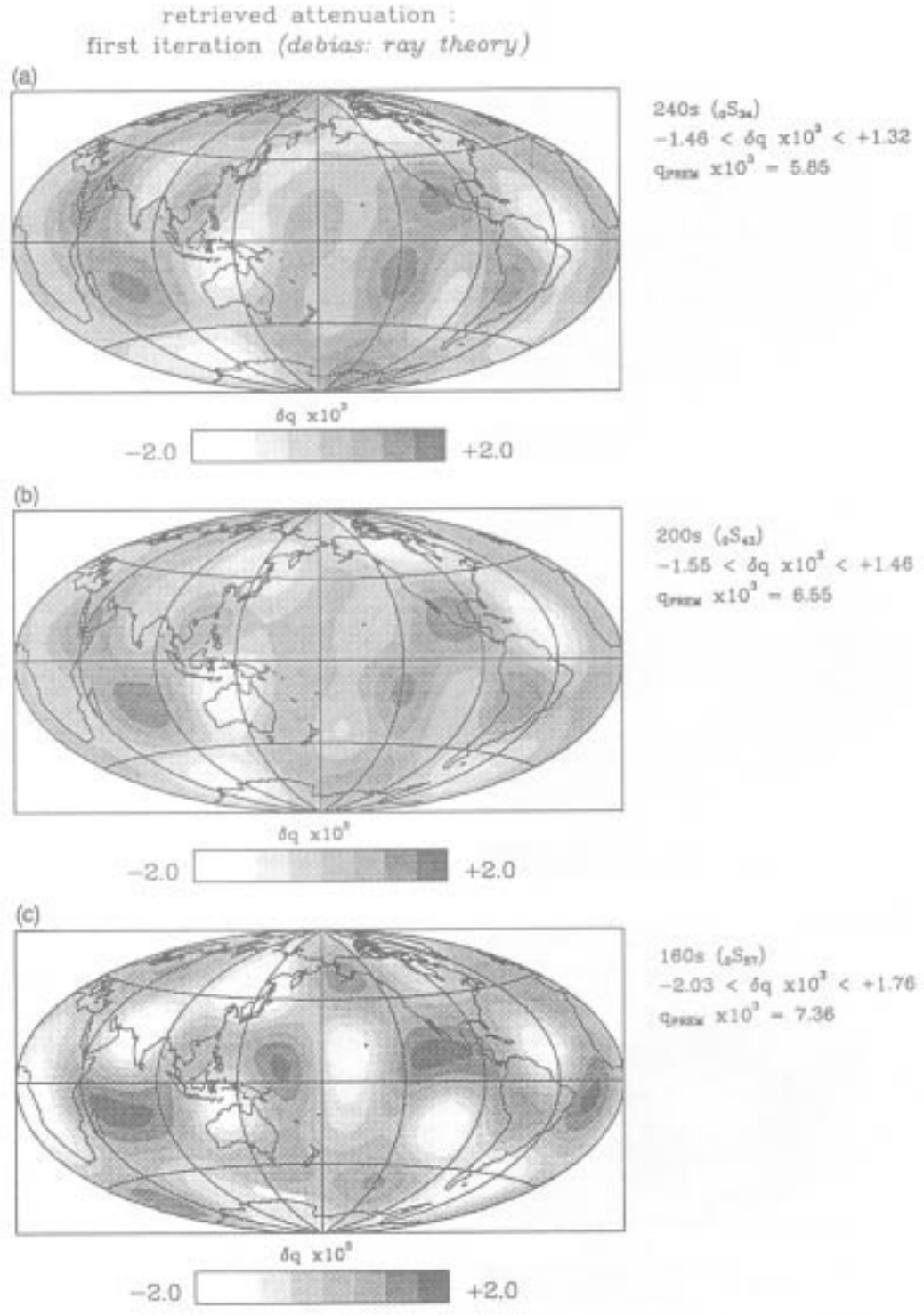

Figure 12. As in Fig. 11 except that the reference velocity-model MPA12.4A and full ray-theoretic expressions were used to predict the remaining elastic bias in the desensitized data.

signal, the inversion is performed for a one layer model of $\alpha(r)$. The layer is unconstrained in location and thickness but is restricted to span at most the whole upper mantle and at least the distance between radial knots in the reference earth model. Figs 18(a) through 18(c) present the suite of one-layer models that nearly equally well explain the retrieved-attenuation coefficients. The length of the line on the plot indicates the depth extent of the single layer. Although allowed in the inversion, models in which the proportionality coefficient is below (approximately) −0.4 violate the physical requirement that the inverse quality factor remain positive; seismic waves are required to attenuate. The striking feature is that all of the models either span or contained in the low-velocity zone. The ray theoretic model of surface wave attenuation yields no values of $\alpha(r)$ which fall below −0.4.

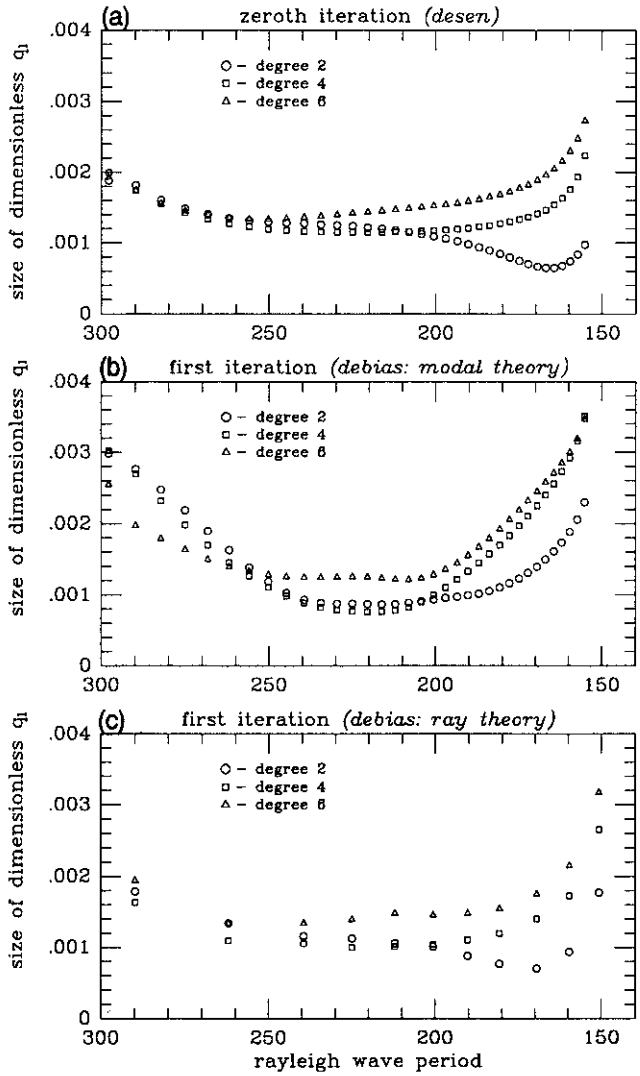

Figure 13. The modulus of the individual degrees in the attenuation expansion, $|\sum_t (q_s^t)^2|^{1/2}$, as a function of period.

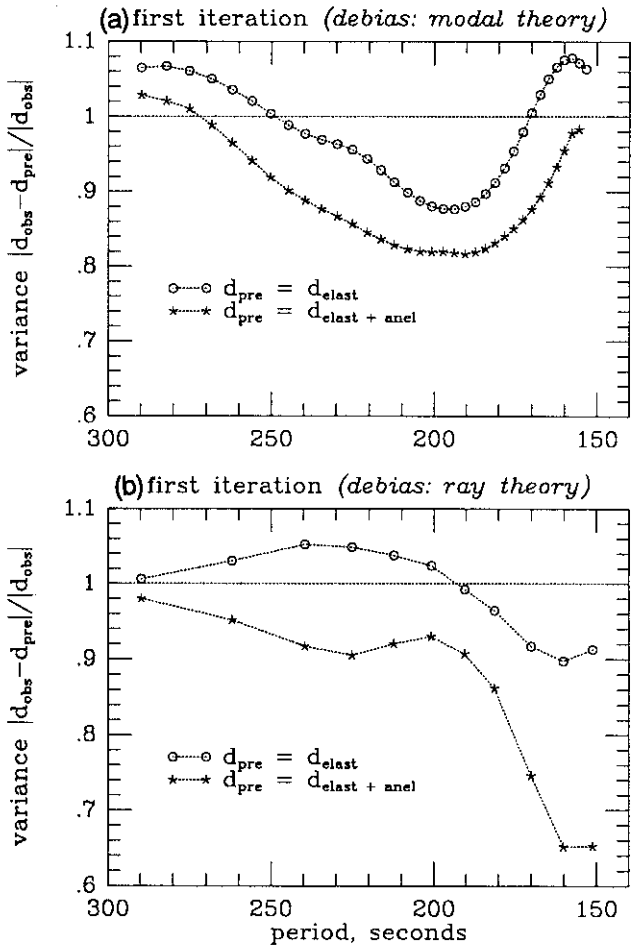

Figure 14. The variance reduction in the desensitized data after the first iteration as yielded by (a) modal theory and (b) ray theory. The upper curve is the variance afforded by the reference elastic model alone while the lower curve includes the variance reduction provided by the addition of anelastic structure. While the normal-mode theory yields a greater reduction near 200 s, ray theory performs better at shorter periods, probably due to the inadequacy of the modal-coupling scheme at higher frequencies.

Examining the radial proportionality factor further, the final inversion considers $\alpha(r)$ to be continuous in the sense that an α_i may be assigned at each radial knot i in the reference earth model. For the radially discrete parameterization of earth models, the integral relationship in eq. (30) is reduced to the sum

$$\delta q_s^t(\omega) = \sum_{n_0}^{n_\oplus} K_i(r_i, \omega)\left[\alpha(r_i)\frac{\delta v_s^t(r_i)}{v(r_i)}\right] r_i^2 \Delta r \qquad (31)$$

leading to a linear system for the discrete proportionality constant, α_i. Smoothness constraints are placed on the first and second derivatives to supress short-wavelength structure in $\alpha(r)$ that is neither supported by the signal-to-noise level of the attenuation coefficients nor physically realistic. The resulting function $\alpha(r)$ in Fig. 19 again presents the striking feature that the source region for anelastic heterogeneity resides in the shallow mantle (100–300 km). The inversion of $\alpha(r)$ for individual degrees is a less stable operation and cannot be confidently performed.

We may evaluate the success of the inversion for $\alpha(r)$ by comparing estimated attenuation maps with those predicted by mapping the elastic reference model through $\alpha(r)$ as presented in eq. (30) and measured by the correlation coefficient in Fig. 20. While the correlations between the retrieved attenuation and phase velocity are poor and straddle zero, the correlation coefficient between the retrieved and predicted surface wave attenuation is significant over most of the period range of interest. Fig. 21 compares the retrieved attenuation model at 200 s period with that predicted by mapping the reference velocity model through the proportionality constant $\alpha(r)$. While the magnitude of the attenuation is underestimated, with only 35 per cent of the variance in the attenuation coefficients explained, the correlation coefficient is 0.69 for 28 coefficients. A proportionality constant between intrinsic velocity and anelasticity that is dominant in the shallow mantle is thus able to explain a significant part of the heterogeneity in surface wave attenuation.

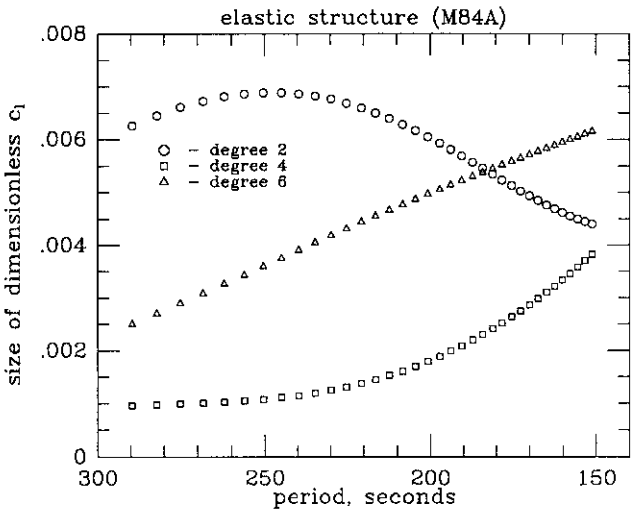

Figure 15. The modulus of the individual degrees of phase velocity as a function of period for the velocity model M84A. The characteristically strong degree 2 transition-zone feature that is evident in the phase velocity is absent in the attenuation models, implying a different source region of anelastic heterogeneity.

DISCUSSION

In this section, we compare the results of this study with previous work and examine the geodynamical implications of our upper mantle anelasticity model. Numerous investigations have documented large-amplitude signals from elastic focusing (e.g. Lay & Kanamori 1985; Woodhouse & Wong 1986), effects large enough to be seen on raw seismograms (Fig. 1). In the extensive study by Romanowicz (1990), the inversion for aspherical attenuation is parameterized to solve explicitly for elastic focusing terms. From 130 carefully selected observations, Romanowicz corroborated Davis's (1985) finding that the amplitude signal from elastic focusing is comparable in size to the signal from aspherical attenuation. The forward-amplitude calculations in Section 3 for realistic elastic and anelastic earth models also confirm the large elastic amplitude signal, and the experimental results make it evident that efforts to constrain anelasticity which neglect elastic signal are irreparably biased.

The synthetic experiments presented in this study reveal that, after applying the linear ray theoretic correction, the residual elastic signal in the data can account for roughly 30 per cent of the retrieved attenuation maps. To address this corrupting elastic signal remaining in the data, we have explicitly predicted and removed the signal using accurate forward theories and recent aspherical elastic models. Romanowicz (1990) also incorporates the principles of linearized ray theory to reduce the elastic signal, but does not explicitly strip remaining elastic signal from the data, citing a lack of confidence in the gradients of the current elastic models, since elastic focusing is a function of the second transverse derivative of the phase velocity along the ray path. Given that the latest generation of elastic models, based on an order of magnitude more data than previous models, appear to be converging and that phase velocity models are more robust than intrinsic velocity models since

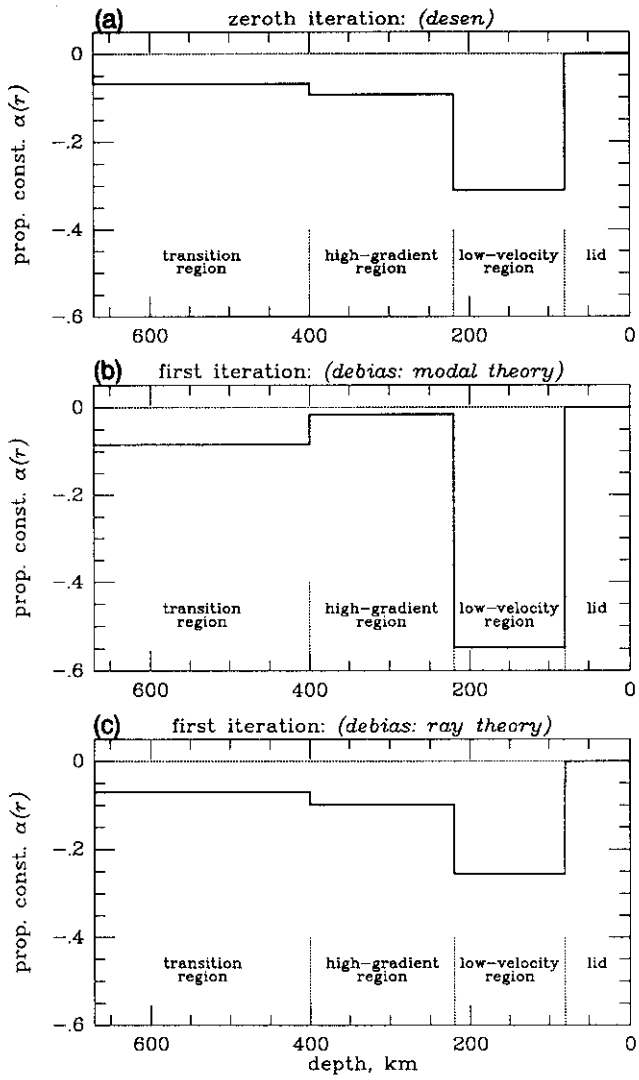

Figure 16. The four-layer proportionality constant $\alpha(r)$ scaling the upper mantle shear velocity to anelasticity after the (a) zeroth iteration and the (b) and (c) first iteration. In all of the cases, the low-velocity zone is the dominant source region for the aspherical-anelastic signal.

they represent the surface projection of radial structure, we argue that it is warranted and necessary to attempt to remove additional elastic signal in the amplitude data explicitly using an elastic reference model. Declining to use a reference aspherical elastic model is actually using one: a purely spherical model. It is difficult to conceive of a spherical elastic model being statistically superior to the current generation of aspherical elastic models with respect to predicting the amplitudes of surface waves.

In considering the radial distribution of anelastic heterogeneity, Romanowicz (1990) observes a long-wavelength correlation between high surface wave phase velocity and low attenuation, although for the low number of degrees of freedom in her models, the peak correlation coefficient of −0.5 may not be statistically significant [in a degree 2 expansion, for instance, a correlation coefficient of −0.5 has a 95 per cent confidence interval of (−0.82, +0.25)]. Based on the correlation between her phase velocity models, which have a known degree 2 source in the

Table 3. The complex harmonic coefficients δq_l^m for the preferred model of Rayleigh-wave attenuation $\delta q(\theta, \phi, \omega)$ at periods of 240, 200 and 160 s. The model was obtained after the first iteration in which the remaining elastic signal in the desensitized data was removed using ray theoretic predictions. The convention of the spherical harmonic expansion is that of Edmonds (1970).

		240s (${}_0S_{34}$)			200s (${}_0S_{43}$)			160s (${}_0S_{57}$)		
l	m	$\delta q_l^m x10^3$	Error	Resolution	$\delta q_l^m x10^3$	Error	Resolution	$\delta q_l^m x10^3$	Error	Resolution
0	0	-.5056	.0684	.9460	-.1822	.0754	.9456	1.8965	.1119	.9442
2	0	-.0791	.1200	.7942	-.5194	.1326	.7928	-.4598	.1964	.7891
2	1	-.2677	.0737	.8591	-.1877	.0817	.8562	-.1111	.1225	.8475
		.3139	-.0820	.8208	.2336	-.0903	.8212	-.5485	-.1332	.8190
2	2	-.0965	.0833	.8125	-.1374	.0915	.8134	-.1196	.1344	.8122
		-.6990	-.0910	.7623	-.5155	-.1002	.7618	-.0746	-.1480	.7581
4	0	.3542	.1368	.7021	.2476	.1511	.7009	.1194	.2234	.6977
4	1	-.3220	.0936	.7515	-.4115	.1037	.7482	-.3519	.1543	.7389
		.4410	-.0969	.6914	.2316	-.1066	.6936	.2255	-.1567	.6961
4	2	.1027	.0878	.7907	.2319	.0969	.7905	.6310	.1432	.7882
		.2457	-.0975	.6949	-.0390	-.1077	.6934	-.4928	-.1592	.6849
4	3	-.2578	.0920	.7562	-.2539	.1012	.7572	-.4671	.1490	.7559
		.1780	-.0966	.7019	.2084	-.1067	.7011	.2319	-.1582	.6954
4	4	.0205	.1027	.6490	.1804	.1132	.6529	-.0604	.1667	.6567
		.1444	-.1000	.6861	.3070	-.1101	.6871	.6330	-.1620	.6857
6	0	.4675	.1445	.6490	.3369	.1596	.6459	-.4110	.2360	.6374
6	1	.0259	.0992	.6967	-.0560	.1097	.6932	.4461	.1627	.6846
		.3810	-.1045	.6143	.3482	-.1151	.6183	.1746	-.1696	.6271
6	2	.1794	.1006	.6721	.2236	.1111	.6709	.2183	.1644	.6668
		.0087	-.1024	.5781	-.0861	-.1128	.5782	-.4463	-.1658	.5750
6	3	.1647	.0980	.7058	.3709	.1080	.7071	.8025	.1592	.7080
		-.1746	-.0970	.7196	-.4024	-.1069	.7177	-.5480	-.1582	.7091
6	4	-.2456	.0993	.6665	-.0445	.1094	.6657	-.0446	.1612	.6629
		.0034	-.1000	.6765	.1171	-.1102	.6768	-.2095	-.1626	.6713
6	5	.4487	.1012	.6663	.3955	.1115	.6680	.3017	.1645	.6681
		-.3507	-.1030	.6553	-.4701	-.1137	.6524	-.0287	-.1680	.6443
6	6	.1538	.1075	.5657	.0972	.1186	.5709	-.2824	.1743	.5788
		.3830	-.1058	.5869	.3516	-.1167	.5866	.7695	-.1720	.5831

mid-upper mantle (250–500 km), and the attenuation models, she concludes that the source region of elastic and anelastic heterogeneity are identical. In contrast, the correlation between the degree 6 surface wave attenuation models of this study and phase velocity models cannot be confidently distinguished from zero. However, phase velocity and attenuation are depth-integrated functions of intrinsic structure and share the same sensitivity kernels. If they are not well correlated, the implication is that the source region of elastic and anelastic heterogeneity are at different depths. From the inversion for the radial proportionality constant between intrinsic velocity and anelasticity (Section 6), the prominent anelastic signal resides in the shallow mantle (100–300 km). While we do not rule out lateral vatiations in Q in the upper mantle below 400 km, they are not required at the level at which we are fitting the data. Thus, the dominant anelastic heterogeneity signal emanates from a shallow source region corresponding roughly with the low-velocity region of PREM.

The decrease in velocity and attenuation in the shallow mantle has been shown to be consistent with both the presence of a small percentage of partial melting and a material just below its solidus temperature (O'Connell and Budianski 1977; Shankland, O'Connell & Waff 1981). O'Connell & Budianski (1977) have demonstrated that fluid flow in cavities introduces an additional mechanism for dissipation, leading to a material in which attenuation is essentially frequency independent. If seismology is confidently able to distinguish the frequency dependence of Q in the low-velocity zone relative to the general mantle, the question of partial melt could be resolved. O'Connell & Budianski (1977) also demonstrate that a sharp boundary definition of the low-velocity zone would argue for the presence of partial melt. However, recent studies have discounted a global discontinuity at 220 km (Shearer 1991) and found it to be an an irregular feature generally observed only below continents (Revenaugh & Jordan 1991; N. Pavlenkova, personal communication).

Combining laboratory and seismic measurements, Sato *et al.* (1988) demonstrate that velocities decrease markedly beyond the solidus temperature but vary weakly at subsolidus temperatures, although sufficiently to explain the low-velocity region without appealing to partial melting. In contrast, the quality factor is a relatively uniform function of temperature across the solidus boundary, but is more

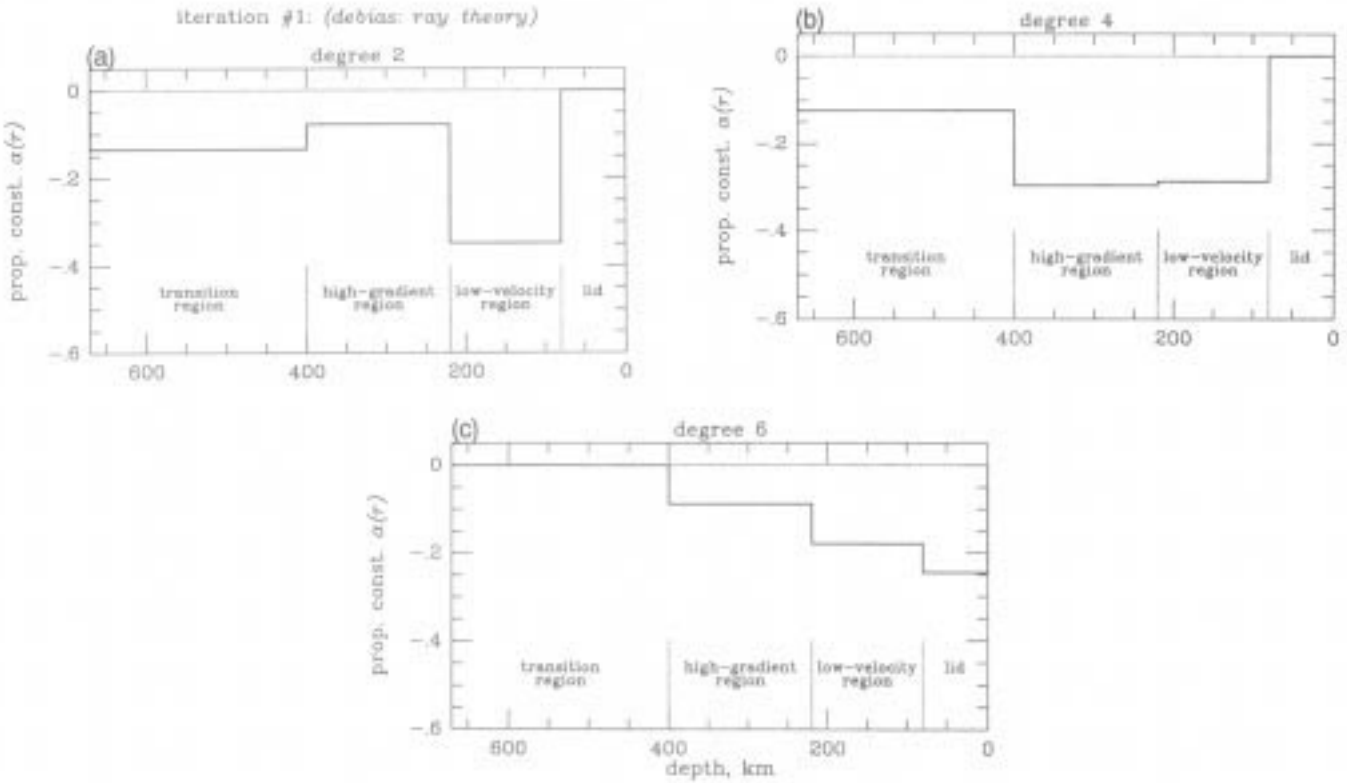

Figure 17. The four-layer proportionality constant $\alpha(r)$ for the individual degrees of the anelastic model from ray theory (Table 3, Fig. 12). The (a) degree 2 anelasticity favours a deeper-source region for anelastic signal while the (b) degree 4 and (c) degree 6 source regions are shallower.

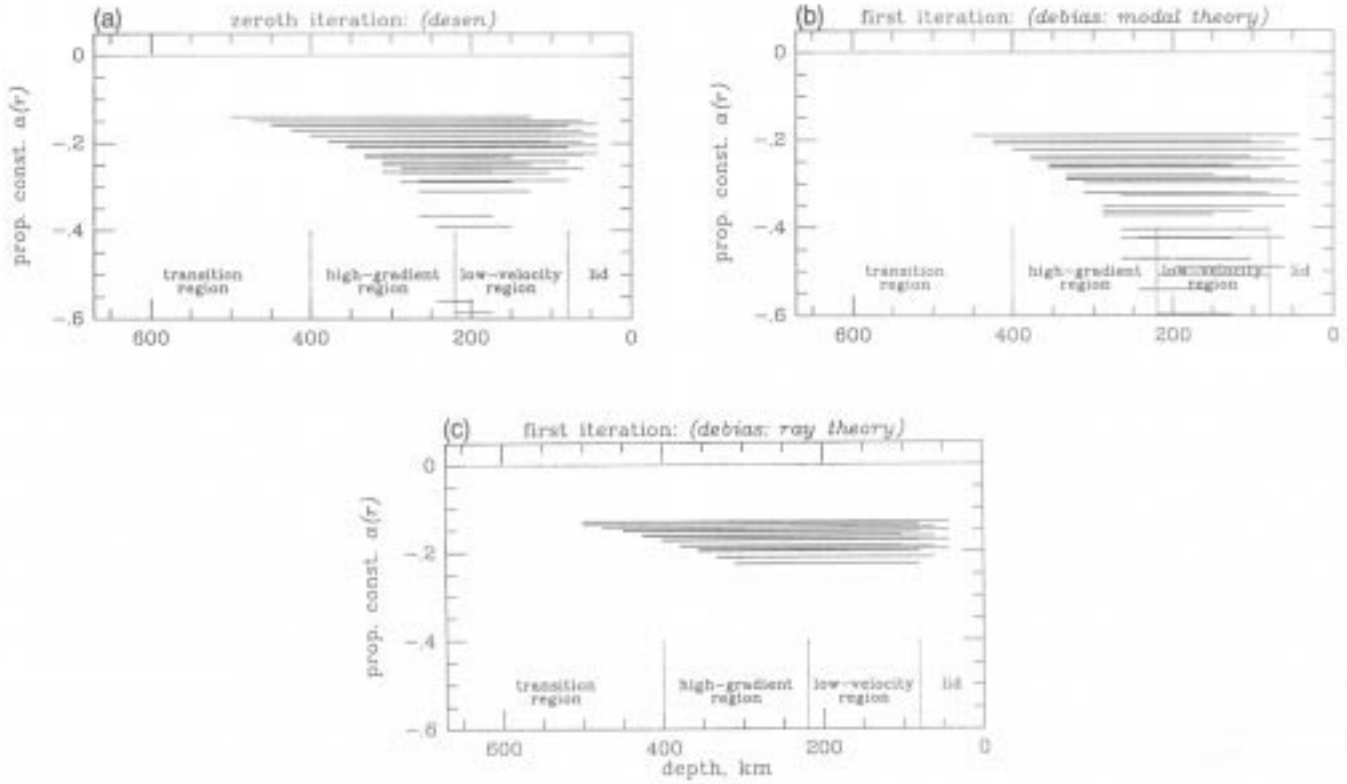

Figure 18. The suite of one-layer models of the proportionality constant $\alpha(r)$ which equally well explain the retrieved attenuation models from the first two iterations. All of the models of $\alpha(r)$ are non-zero within some or all of the low-velocity zone. In Fig. (c), all of the values of $\alpha(r)$ are greater than -0.4, the approximate value below which waves would grow instead of dissipate.

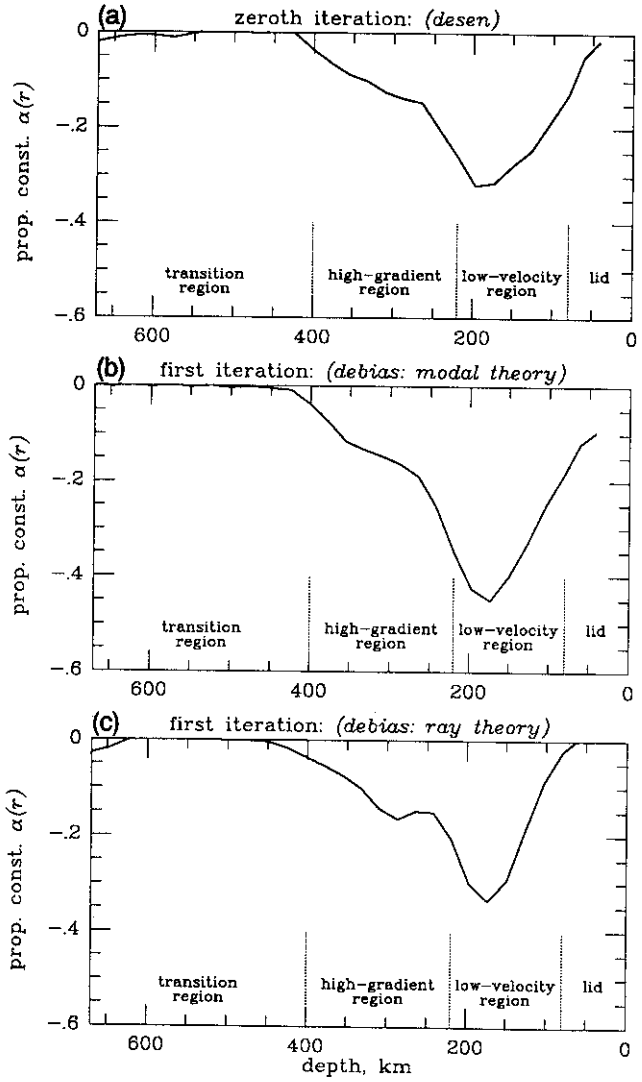

Figure 19. The smooth proportionality constant $\alpha(r)$ for the retrieved anelasticity after the first two iterations. The dominant source region of anelastic signal is the low-velocity zone.

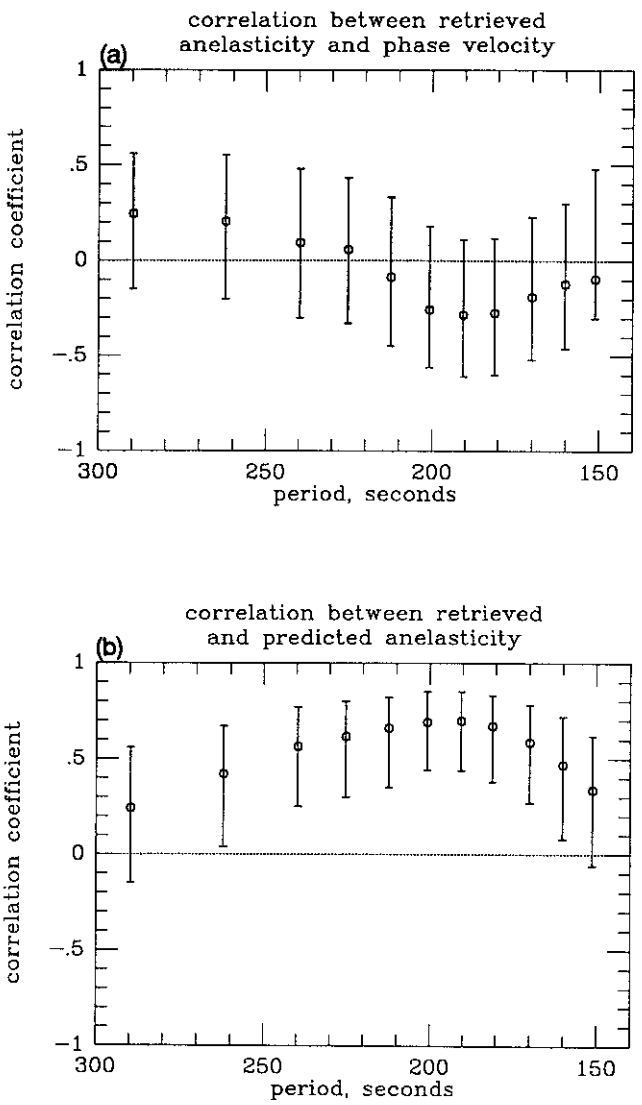

Figure 20. Phase velocity and surface wave attenuation are poorly correlated as demonstrated in (a) in which the correlation coefficient straddles zero. Fig. (b) demonstrates the high correlation between the retrieved-attenuation models and the predicted attenuation obtained by mapping shear velocity model M84A through $\alpha(r)$. The brackets denote the 95 per cent confidence interval.

strongly sensitive to temperature variations below the solidus than velocity (Sato *et al.* 1988). Given that lateral velocity variations in the low-velocity zone are comparable in size to those of the surrounding mantle, the results of this study, which show anomalously strong anelastic heterogeneity in the low-velocity zone, appear most consistent with a material which lies near, but below, the solidus temperature.

CONCLUSIONS

In this study, we have utilized an unbiased datum constructed from surface wave amplitude anomalies to constrain even-degree heterogeneity in surface wave attenuation. The retrieved attenuation models, in Figs 8–11, reveal that the inverse quality factor Q^{-1} varies by roughly 30 per cent for Rayleigh waves at a period of 200 s.

This study has provided a preliminary understanding of the geometry and radial distribution of intrinsic anelasticity in the upper mantle, but further work is required in increasing and refining our knowledge of intrinsic anelastic structure. As a possible continuation of the technique here, the surface wave attenuation maps obtained in this study may be fixed and the residual signal inverted for refinements to the elastic models, representing the next step in a larger iterative problem. A preferable approach for future studies will combine phase and amplitude information in a simultaneous inversion for elastic and anelastic structure using partial derivative matrices which are sensitive to odd degree structure.

ACKNOWLEDGMENTS

The authors are indebted to Yun Wong who provided his extensive set of amplitude-anomaly measurements. Göran Ekström and Adam Dziewonski provided critical questions and discussions. Barbara Romanowicz supplied a preprint of

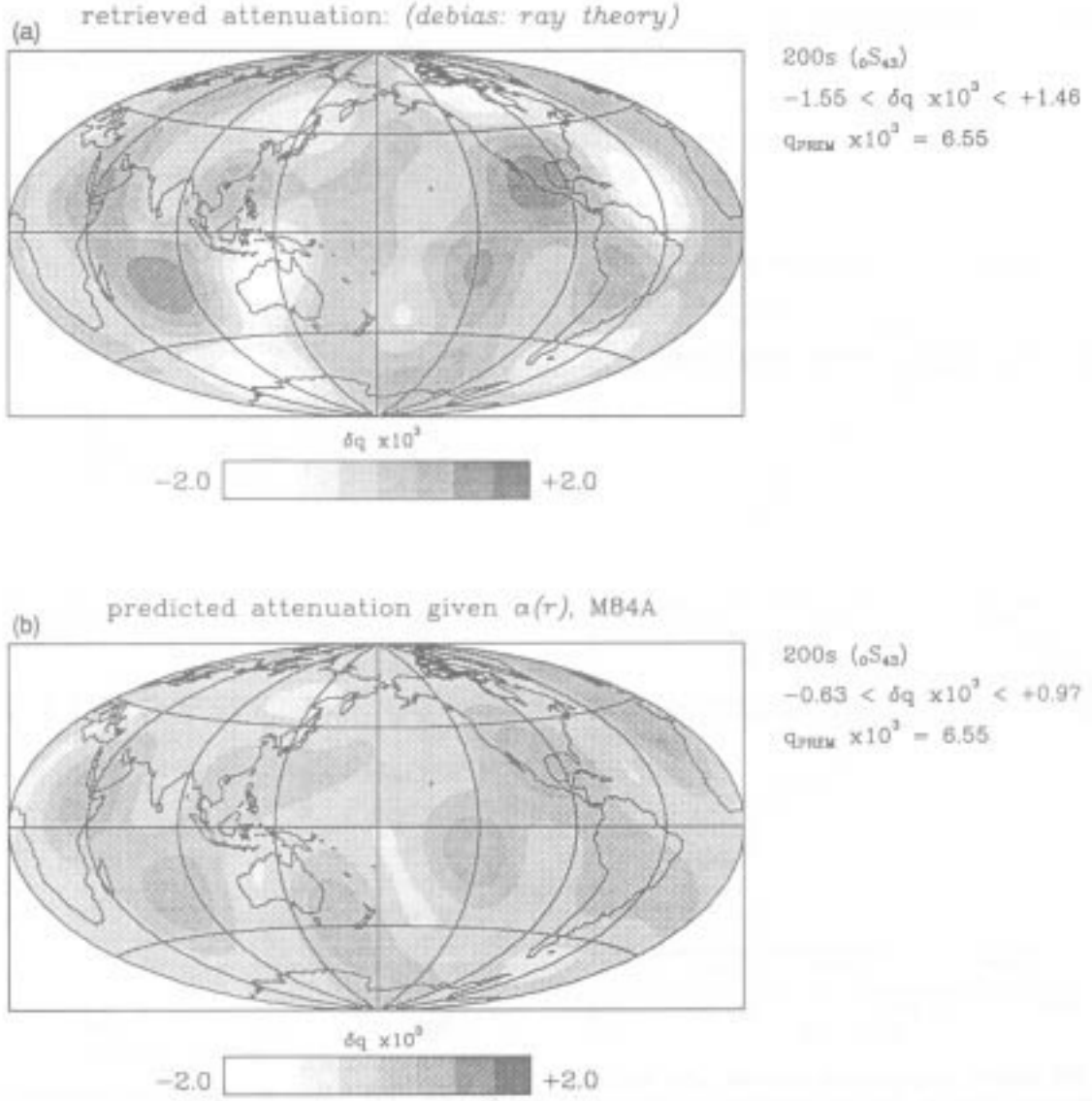

Figure 21. Maps of retrieved and predicted surface wave attenuation at a period of 200 s, further demonstrating the ability of a shear velocity model mapped through a proportionality constant which is dominant in the low-velocity zone to explain the observed surface wave attenuation. While the retrieved model is underpredicted, with a variance reduction of 35 per cent, the correlation coefficient is 0.69 for 28 model coefficients.

her attenuation study. We thank Jeremy Bloxham and Rick O'Connell who generously devoted computer time on their Sun-4 workstations at a crucial juncture in these experiments. This study was supported by the National Science Foundation Grant EAR-872-1301 as well as NSF supercomputing grants *ylw* and *xfo* at the National Center for Supercomputing Applications, University of Illinois, Urbana–Champaign. Joseph Durek was supported by a National Science Foundation Graduate Fellowship and National Science Foundation Grant EAR-9105531.

REFERENCES

Backus, G. E., 1964. Geographical interpretation of measurements of average phase velocities of surface waves over great circular and great semi-circular paths, *Bull. seism. Soc. Am.*, **54,** 571–610.

Backus, G. E. & Gilbert, F., 1967. Numerical applications of a formalism for geophysical inverse problems, *Geophys. J. R. astr. Soc.*, **13,** 247–276.

Backus, G. E. & Gilbert, F., 1968. The resolving power of gross earth data, *Geophys. J. R. astr. Soc.*, **16,** 169–205.

Backus, G. E. & Mulcahy, M., 1976. Moment tensors and other phenomenological descriptions of seismic sources, II. Discontinuous displacements, *Geophys. J. R. astr. Soc.*, **47,** 301–330.

Ben-Menahem, A., 1965. Observed attenuation and Q values of seismic surface waves in the upper mantle, *J. geophys. Res.*, **70,** 4641–4651.

Dahlen, F. A., 1987. Multiplet coupling and the calculation of synthetic long-period seismograms, *Geophys. J. R. astr. Soc.*, **91,** 241–254.

Davis, J. P. 1985. Variation in apparent attenuation of the Earth's normal modes due to lateral heterogeneity, *Geophys. Res. Lett.*, **12,** 141–143.

Davis, J. P. & Henson, I. H., 1986. Validity of the great circle average approximation for inversion of normal mode measurements, *Geophys. J. R. astr. Soc.*, **85,** 69–92.

Durek, J. J., Dziewonski, A. M. & Woodhouse, J. H., 1988. Even order global distribution of the quality factor Q by inversion of surface wave amplitude data, *EOS Trans. Am. geophys. Un.*, **69,** 397.

Durek, J. J., Ritzwoller, M. H. & Woodhouse, J. H., 1989. Estimating aspherical Q in the upper mantle using surface wave amplitude data, *EOS Trans. Am. geophys. Un.*, **70,** 1212.

Dziewonski, A. M. & Anderson, D. L., 1981. Preliminary reference earth model (PREM), *Phys. Earth planet. Inter.*, **25,** 297–356.

Dziewonski, A. M., Chou, T.-A. & Woodhouse, J. H., 1981. Determination of earthquake source parameters from waveform data for studies of global and regional seismicity, *J. geophys. Res.*, **86,** 2825–2852.

Dziewonski, A. M. & Steim, J. M., 1982. Dispersion and attenuation of mantle waves from waveform inversion, *Geophys. J. R. astr. Soc.*, **70,** 503–527.

Edmonds, A. R., 1960. *Angular Momentum in Quantum Mechanics*, Princeton University Press, Princeton, New Jersey.

Gubbins, D. & Bloxham, J., 1985. Geomagnetic field analysis—III: magnetic fields on the core–mantle boundary, *Geophys. J. R. astr. Soc.*, **80,** 695–713.

Jackson, D. D., 1979. The use of *a priori* data to resolve non-uniqueness in linear inversion, *Geophys. J. R. astr. Soc.*, **57,** 137–157.

Jobert, N. & Jobert, G., 1983. An application of ray theory to the propagation of waves along a laterally heterogeneous spherical surface, *Geophys. Res. Lett.*, **10,** 1148–1151.

Jordan, T. H., 1978. A procedure for estimating lateral variations from low-frequency eigenspectra data, *Geophys. J. R. astr. Soc.*, **52,** 441–455.

Kanamori, H., 1970. Velocity and Q of mantle waves, *Phys. Earth planet. Inter.*, **2,** 259–275.

Lay, T. & Kanamori, H., 1985. Geometric effects of global lateral heterogeneity on long period surface wave propagation. *J. geophys. Res.*, **90,** 605–621.

Masters, G. & Gilbert, F., 1983. Attenuation in the Earth at low frequencies, *Phil. Trans. R. Soc. Lond.*, A, **308,** 479–522.

Masters, G., Jordan, T. H., Silver, P. G. & Gilbert, F., 1982. Asperical earth structure from fundamental spheroidal-mode data, *Nature*, **298,** 609–613.

Mills, J. M., 1978. Great circle Rayleigh wave attenuation and group velocity. Part IV: regionalization and pure-path models for shear velocity and attenuation, *Phys. Earth planet. Inter.*, **17,** 323–352.

Nakanishi, I., 1979. Phase velocity and Q of mantle rayleigh waves, *Geophys. J. R. astr. Soc.*, **58,** 35–59.

Nakanishi, I. & Anderson, D. L., 1983. Measurements of mantle wave velocities and inversion for lateral heterogeneity and anisotropy. I: analysis of great circle phase velocities, *J. geophys. Res.*, **88,** 10267–10283.

Nakanishi, I. & Anderson, D. L., 1984. Measurements of mantle wave velocities and inversion for lateral heterogeneity and anisotropy. II: analysis by the single-station method, *Geophys. J. R. astr. Soc.*, **78,** 573–617.

O'Connell, R. J. & Budianski, B., 1977. Viscoelastic properties of fluid saturated and cracked solids, *J. geophys. Res.*, **82,** 5719–5735.

O'Connell, R. J. & Budianski, B., 1978. Measures of attenuation in dissipative media, *Geophys. Res. Lett.*, **5,** 5–8.

Park, J., 1987. Asymptotic coupled-mode expressions for multiplet amplitude anomalies and frequency shifts on an aspherical Earth, *Geophys. J. R. astr. Soc.*, **90,** 129–169.

Park, J. & Gilbert, F., 1986. Coupled free oscillations of an aspherical, dissipative, rotating Earth: Galerkin theory, *J. geophys. Res.*, **91,** 7241–7260.

Pollitz, F. F., Park, J. & Dahlen, F. A., 1987. Observations of free oscillation amplitude anomalies, *Geophys. Res. Lett.*, **14,** 895–898.

Revenaugh, J. & Jordan, T., 1991. Mantle layering from *ScS* reverberations 3. The upper mantle, *J. geophys. Res.*, **96,** 19 781–19 810.

Ritzwoller, M., Masters, G. & Gilbert, F., 1988. Constraining aspherical structure with low frequency interaction coefficients: application to uncoupled multiplets, *J. geophys. Res.*, **93,** 6369–6396.

Ritzwoller, M. H., Durek, J. J. & Woodhouse, J. H., 1989. Inferences from measurements of aspherical Q, *EOS. Trans. Am. geophys. Un.*, **70,** 1212.

Romanowicz, B., 1987. Multiplet–multiplet coupling due to lateral heterogeneity: asymptotic effects on the amplitude and frequency of the Earth's normal modes, *Geophys. J. R. astr. Soc.*, **90,** 75–100.

Romanowicz, B., 1990. The upper mantle degree 2: constraints and inferences from global mantle wave attenuation measurements, *J. geophys. Res.*, **95,** 11 051–11 071.

Romanowicz, B., Ekström, G. & Lognonné, P., 1989. On how to handle focussing effects in long period Rayleigh wave attenuation measurements, *EOS. Trans. Am. geophys. Un.*, **70,** 1186.

Romanowicz, B., Roult, G. & Kohl, T. 1987. The upper mantle degree two pattern: constraints from GEOSCOPE fundamental spheroidal mode eigenfrequency and attenuation measurements, *Geophys. Res. Lett.*, **14,** 1219–1222.

Roult, G., 1982. The effect of young oceanic regions on frequencies and damping of free oscillations of the Earth, *J. Geophys.*, **51,** 38–43.

Sailor, E. M. & Dziewonski, A. M., 1978. Measurements and interpretation of normal mode attenuation, *Geophys. J. R. astr. Soc.*, **53,** 559–581.

Sato, Y., 1958. Attenuation, dispersion and the wave guide of the G wave, *Bull. seism. soc. Am.*, **48,** 231–251.

Sato, H., Sacks, I. S., Murase, T. & Scarfe, C. M., 1988. Thermal structure of the low velocity zone derived from laboratory and seismic investigations, *Geophys. Res. Lett.*, **15,** 1227–1230.

Shankland, T. J., O'Connell, R. J. & Waff, H. S., 1981. Geophysical constraints on partial melt in the upper mantle, *Rev. Geophys. & Space Phys.*, **19,** 394–406.

Shearer, P., 1991. Constraints on upper-mantle discontinuities from observations of long-period reflected and converted phase, *J. geophys. Res.*, **96,** 18147–18182.

Sipkin, S. A. & Jordan, T. H., 1980. Regional variation of Q_{ScS}, *Bull. seism. Soc. Am.*, **70,** 1071–1102.

Smith, M. F. & Masters, G., 1989. Aspherical structure constraints from normal mode frequency and attenuation measurements, *J. geophys. Res.*, **94,** 1953–1976.

Tanimoto, T., 1985. The Backus–Gilbert approach to the three-dimensional structure in the upper mantle, I. Lateral variation of surface wave phase velocity with its error and resolution, *Geophys. J. R. astr. Soc.*, **82,** 105–124.

Tanimoto, T., 1986. The Backus–Gilbert approach to the three-dimensional structure in the upper mantle, II. *SH* and *SV* velocity, *Geophys. J. R. astr. Soc.*, **84,** 105–124.

Tarantola, A. & Valette, B., 1982. Generalized non-linear inverse problems solved using the least squares criterion, *Rev. Geophys. Space Phys.*, **20,** 219–232.

Wong, Y. K., 1989. Upper mantle heterogeneity from phase and amplitude data of mantle waves, *PhD thesis*, Harvard University, Cambridge.

Woodhouse, J. H., 1974. Surface waves in a laterally varying layered structure, *Geophys. J. R. astr. Soc.*, **37,** 461–490.

Woodhouse, J. H., 1980. The coupling and atteneuation of nearly resonant multiplets in the Earth's free oscillation spectrum, *Geophys. J. R. astr. Soc.*, **61,** 261–283.

Woodhouse, J. H. & Dahlen, F. A., 1978. The effect of a general aspherical perturbation on the free oscillations of the Earth, *Geophys. J. R. astr. Soc.*, **53,** 335–354.

Woodhouse, J. H. & Dziewonski, A. M., 1984. Mapping the upper mantle: three-dimensional modeling of earth structure by inversion of seismic waveforms, *J. geophys. Res.*, **89,** 5953–5986.

Woodhouse, J. H. & Girnius, T. P., 1982. Surface waves and free oscillations in a regionalized Earth model, *Geophys. J. R. astr. Soc.*, **68,** 653–673.

Woodhouse, J. H. & Wong, Y. K., 1986. Amplitude, phase and path anomalies of mantle waves, *Geophys. J. R. astr. Soc.*, **87,** 753–773.